ADVANCED MATERIALS TECHNOLOGIES
www.advmattechnol.de

Recent Developments in Graphene-Based Tactile Sensors and E-Skins

Shuai Chen, Kai Jiang, Zheng Lou, Di Chen,* and Guozhen Shen**

Human skin, the largest organ of human body, can perceive tactile sensations, temperature, humidity, and other complex environmental stimulations. To mimic the capabilities of human skin, graphene provides great potential in building wearable electronic skins (E-skins), which hold broad applications in advanced robotics, healthcare monitoring, artificial intelligence, human–machine interfaces, etc. Herein, the recent progress in flexible tactile sensors and E-skins based on graphene material is presented. A brief introduction of the main approaches to prepare graphene nanosheets is provided. The main developments on the functions and mechanisms of bionic functional devices in E-skins including tactile sensors, temperature sensors, and humidity sensors are then highlighted. The current and future applications for graphene-based E-skins, such as multifunctional biomimetic E-skins, healthcare monitoring, and interactive human–machine interface, are also described. Finally, the existing challenges and future development trends for graphene-based E-skins are discussed.

1. Introduction

The development of electronic skins (E-skins) for the mimicry of human sensory system has drawn great attentions recently, which has a great potential in the applications of artificial intelligence, healthcare monitoring, artificial prosthesis, and human–machine interaction electronics.[1–4] Human skin, served as the largest sensory organ in human body, can help us communicate with surroundings such as the contacted pressures, changed temperatures, shapes, and textures of touched objects, via the specialized sense receptors.[5,6] For an intact haptic system, the collected information will be sent to the central nervous systems for comprehending and processing the meaning of the received information, and then our body will be guided to respond to the physical contact successfully. To imitate the sophisticated perception of human skin, various kinds of functional electronic devices which can sense and distinguish external physical, chemical, and biological signals simultaneously are integrated in a flexible or elastic system likes human skin. The functional electronic devices including pressure sensor, temperature sensor, and humidity sensor[7–9] have the ability to transfer the generated information from physical signals into electrical signals that electronic devices can recognize.[10–12] However, there remains enormous challenges to construct E-skins with multimodal detection, fleet response, high sensitivity and resolution, even though much research has been reported on the imitation of human skin behaviors recently.

The rise of E-skins in early years may be resulted from the inspiration of science fiction and movies, which builds a bridge between virtual imagination and scientific reality. Since a prosthetic hand with tactile feedback was demonstrated by Clippinger et al. in 1974,[13] several studies have been followed to explore the potential application of tactile bionics.[14–16] Especially, flexible electronics achieved significant progress which served as a foundation to construct E-skins, due to the particular importance of mechanical compliance and highly sensitive characteristics in mimicking human skin.[17–21] For examples, Rogers and co-workers developed flexible electronics technologies to transfer traditional Si electronic devices onto 100 nm ultrathin films connected by stretchable interconnects.[22,23] Someya and co-workers integrated a large-scale organic field-effect transistors (FETs) based on flexible pentacene which showed excellent pressure sensitivity.[24] Bao and coworkers developed novel self-healing and mechanical force sensing E-skins with microstructured elastomeric dielectrics.[25–27] In addition, piezoresistive, capacitive, and piezoelectric sensors are deemed as three major transduction mechanisms for the

S. Chen, Prof. D. Chen
School of Mathematics and Physics
University of Science and Technology Beijing
Beijing 100083, China
E-mail: chendi@ustb.edu.cn
S. Chen, Dr. Z. Lou, Prof. G. Z. Shen
State Key Laboratory for Superlattices and Microstructures
Institute of Semiconductors
Chinese Academy of Sciences
Beijing 100083, China
E-mail: gzshen@semi.ac.cn
Prof. K. Jiang
Institute & Hospital of Hepatobiliary Surgery
Key Laboratory of Digital Hepatobiliary Surgery of Chinese PLA
Chinese PLA Medical School
Chinese PLA General Hospital
Beijing 100853, China
E-mail: jiangk301@126.com
Prof. G. Z. Shen
College of Materials Science and Opto-Electronic Technology
University of Chinese Academy of Sciences
Beijing 100029, China
The ORCID identification number(s) for the author(s) of this article can be found under https://doi.org/10.1002/admt.201700248.

DOI: 10.1002/admt.201700248

tactile sensors in E-skins, improving the performance of flexible electronic devices.[12,28] On the basis, flexible sensor arrays with a large-scale integration have been fabricated without pixels interferences which promote a high resolution for distributed pressure mapping precisely.[29,30] Meanwhile, the device sensitivity, detected range, scale size, and spatial resolution have immense improvements with the development of materials science, flexible electronics, and nanotechnology, even surpassed the performance of human skin.[31,32] A great breakthrough is the emergence of multifunctional intelligent E-skins which can distinguish various physical stimulation simultaneously, such as pressure, strain, twist, humidity, and temperature changes from the complex external environment.[33,34] Next-generation E-skins with self-healing, self-powered, and artificial intelligent abilities are in continuous evolution.

Except for the real-time monitoring of diversified signals in surrounding environment, E-skins also provide great potential in the medical applications such as human health monitoring.[35,36] For instance, E-skins have been used not only to guide the effective disease precaution and diagnosis via detecting human physiological signals such as pulse checking, electrocardiogram and electroencephalogram monitoring,[37–39] but also to evaluate the human motion status and record the body sports injury via detecting the joint and body motions.[15,40,41] We believe next-generation intelligent E-skins will pave a way to realize the monitoring of external stimulation and corresponding processing as well as responding like authentic haptic system. Therefore, developments of E-skins expand broad applications in humanoid robots, intelligent prosthesis, and smart medical diagnosis, etc.

Although traditional functional sensors have been broadly investigated to mimic the features of human skin, highly flexible devices based on brittle sensing materials yet cause a damage of device structure and performance if using conventional sensor configurations. Nowadays, E-skins based on 1D (e.g., carbon nanotubes (CNTs), metal nanowires (NWs), polymer nanofibers, and inorganic semiconductor nanowires) and 2D (e.g., graphene and MoS_2) materials have been reported, focusing on the application of flexible electronics.[42–45] However, simultaneous realization of high compliance and high sensitivity is still a great challenge because of the materials mismatch at interfaces between low Young's modulus skin and high Young's modulus nanomaterials, which resulted in inaccurate detected signals. In addition, for the transparent and stretchable (TS) devices based on conventional materials, it usually requires a very thin conductive film as electrodes and active layer, which may cause structural cracking or breakage upon applying a strain–stress. The materials with multiaxial stretching ability are required to design isotropous stretchable devices. Another challenge is to achieve large-scale production of 1D-based electronics in practical applications, because of the difficulty to acquire the same level of precision, uniformity, and scalability as well as lab-scale level. Therefore, further studies are needed to achieve flexible and stretchable devices with much higher reliability, durability, and robustness. Graphene, as a novel 2D carbon nanomaterial, possesses excellent characteristics which are required for E-skins, such as the good electrical property, high thermal conductivity, chemical stability, and good mechanical strength.[46,47] The above superiorities reveal a great importance in building flexible E-skins. For instance, graphene-based E-skin is endowed a good mechanical stability while stretched, compressed or twisted, and a preferred component to design device structures for the performance optimization.[48,49] Therefore, E-skins based on graphene have achieved a prominent progress in the past several years as shown in **Figure 1**.

In this review, we focus on the recent progress in flexible tactile sensors and E-skins based on graphene. First, we take a brief introduction to the main approaches to prepare graphene materials. Then, we highlight the main developments on the functions and mechanisms of bionic functional devices

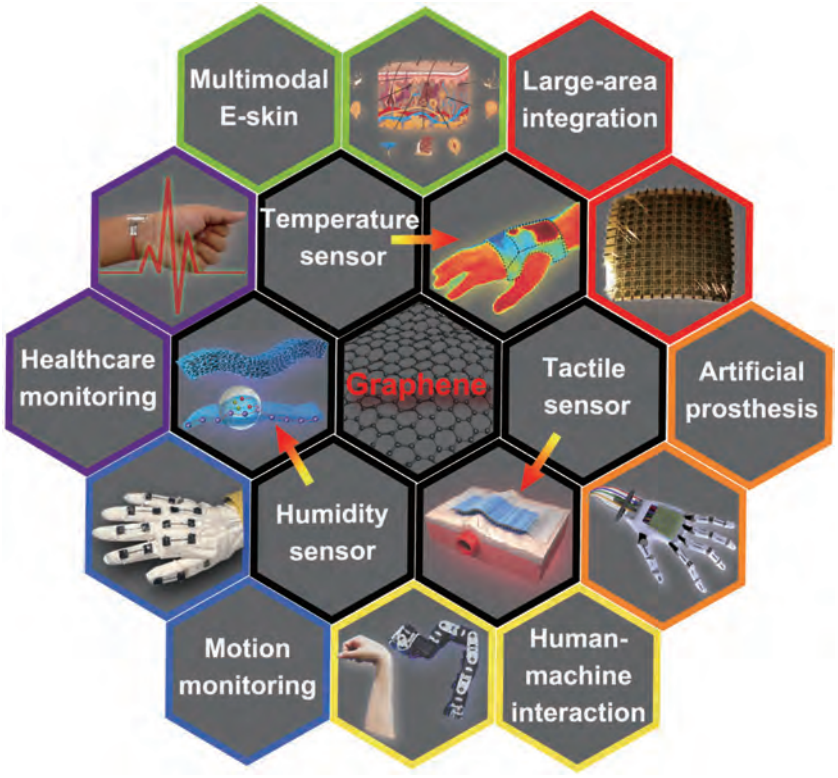

Figure 1. Characteristic categories and diverse applications of recently developed devices for E-skins based on graphene. "Tactile sensor:" Reproduced with permission.[31] Copyright 2014, Wiley-VCH; "Temperature sensor:" Reproduced with permission.[50] Copyright 2016, Wiley-VCH; "Humidity sensor:" Reproduced with permission.[51] Copyright 2017, Wiley-VCH. "Multimodal E-skin:" Reproduced with permission.[52] Copyright 2016, Wiley-VCH. "Healthcare monitoring:" Reproduced with permission.[53] Copyright 2014, Macmillan Publishers Ltd. "Motion monitoring:" Reproduced with permission.[54] Copyright 2011, Macmillan Publishers Ltd. "Human–machine interaction:" Reproduced with permission.[55] Copyright 2014, Wiley-VCH. "Artificial prosthesis:" Reproduced with permission.[56] "Large-area integration:" Reproduced with permission.[57] Copyright 2016, Macmillan Publishers Ltd.

in E-skins, including tactile sensors, temperature sensors, and humidity sensors. We also describe the current and future applications for graphene-based E-skins, such as multifunctional biomimetic E-skins, healthcare monitoring, and interactive human–machine interface. Finally, we discuss the existing challenges and future development trends for graphene-based E-skins.

2. Preparation and Properties of Graphene

Recently, graphene has received significant attention as one ideal material to construct E-skins since its discovery by Novoselov et al. in 2004.[58] As a 2D sheet consists of a honeycomb lattice of sp^2-bonded carbon atoms, graphene holds unique physical properties such as high carrier mobility, excellent electrical and thermal conductivities, high mechanical behavior, a tunable band gap, compared with other carbon allotropes (e.g., carbon nanotubes, graphite, and fullerenes). In electricity, the electrons and holes in graphene with a concentration of up to 10^{13} cm^{-2} exhibit high room-temperature mobility of ≈10 000 cm^2 V^{-1} s^{-1} and low temperature mobility of 200 000 cm^2 V^{-1} s^{-1}. In mechanics, the excellent mechanical properties of graphene with fracture strains of up to 25% and a Young's modulus of ≈1.1 TPa provide a significant opportunity for the applications in flexible and stretchable E-skins. As a vital evaluation parameter of conductivity, the monolayer graphene possesses extremely low sheet resistance of 30 Ω sq^{-1} in theoretical value, while its transparency is up to 97.7%. Several recent reviews[59–61] have discussed the physical properties of graphene in detail; thus, we will only highlight the related preparation method and potential applications of graphene in E-skins here.

Although the outstanding properties of graphene indicate a potential future in various fields, the realization of actual behavior of graphene is difficult to reach the theoretic state. The reasons can be attributed to the imperfection of existing preparation methods, where different methods may lead to obvious differences of the fabricated graphene properties. Recently, two primary methods to fabricate low-cost and large-scale graphene are chemical vapor deposition (CVD) method and solution processed method, which are beneficial for the construction of graphene-based E-skins.

2.1. Chemical Vapor Deposition Growth

The CVD method is an effective approach to achieve high-quality and high-homogeneous graphene films on metal substrates. The growth can be summarized as three steps: the dissolution of carbon atoms into a metal substrate at growth temperature, the precipitation of carbon out of the metal substrate due to the reduction in solubility in cooling stage, and the generation of graphene layers on the surface of metal substrate (**Figure 2**a,b).[62,63] Here, the metals such as Fe, Ni, Co, Ir, Pt, Cu, and Ni–Mo alloy serve as both catalyst and substrate to grow graphene layers. Among them, metals (e.g., Fe, Ni, and Co) with a relatively high solubility of carbon atoms are usually designed to prepare multilayer graphene films, and metals (e.g., Pt and Cu) with a relatively low solubility of carbon atoms are used to produce predominantly single-layer graphene.[64,65] Unfortunately, the conventional CVD process usually requires a high temperature which is difficult for large-scale industrial production. The surface of graphene generated by the direct growth method on flexible substrates often suffers from a mechanical deformation and destruction.[66] Therefore, plasma-enhanced CVD (PECVD) was developed which can decrease the growth temperature as low as 300 °C through combining thermal and plasma energy, thus enabled the direct growth of graphene on a flexible plastic substrates.[67] In addition, Cho and co-workers reported a rapid thermal CVD method which overcame the challenges of hydrogen-free growth to produce homogeneous graphene films over a large area (400×300 mm^2) with a sheet resistance of ≈250 Ω sq^{-1}.[68] Interestingly, selecting liquid metals (e.g., liquid Ga, Cu, and In) as catalyst substrates is a new strategy to fabricate homogeneous graphene film with controllable layer number and crystallinity, owing to the atomic smooth and ultrauniform of liquid metals.[69,70]

The effective strategy for graphene preparation is to generate graphene directly on the required substrates, such as the low-temperature growth on flexible plastic substrate by PECVD. Nevertheless, the drawback of this method is the inferior properties of as-prepared graphene compared to those prepared by conventional CVD at high temperature. As a result, it is necessary to develop effective transfer technologies for CVD-grown graphene to optional substrates for further assembly of electronic devices. The chemical wet-etching method to remove the metallic support is a mature technology now which will not lead to defect formation and property degradation during the transfer of graphene.[71–73] Hong and co-workers utilized the method of roll-to-roll production and wet-chemical doping to transfer large-area (30 in.) monolayer graphene film onto flexible target substrates (Figure 2c–e).[74] The transfer process includes adhesion of graphene films onto polymer supports (e.g., poly(methylmethacrylate) (PMMA) and polydimethylsiloxane (PDMS)), copper etching by electrochemical reaction with ammonium persulfate solution, and transfer printing on a target substrate by removing the adhesive force. At last, the transferred graphene films attached steadily onto required substrates with the retained continuity via van Der Waals forces and π–π interactions. The transferred graphene films held a low sheet resistance (≈125 Ω sq^{-1}) and high optical transmittance (≈97.4%) with excellent resistibility to high strain. However, the roll-to-roll method is not suitable for transferring graphene onto rigid substrates including wafers and glass; due to that, the triggered large mechanical defects on graphene films may lead to the degradation of performance. Choi and co-workers developed an improved dry transfer method taking advantage of hot-pressing technique to reduce mechanical damage through neutralizing mechanical stress (Figure 2f–h).[75] This method could enhance the transfer efficiency of graphene films on rigid substrates with discretionary thickness and rigidity. Recent researches on the CVD growth and transfer of graphene have achieved great progress to obtain high-quality graphene with less contamination and high continuity in a large-scale substrate. Nevertheless, more advanced technologies for solving the challenges such as high cost and complex operation are demanded imminently to expand the large-scale application.

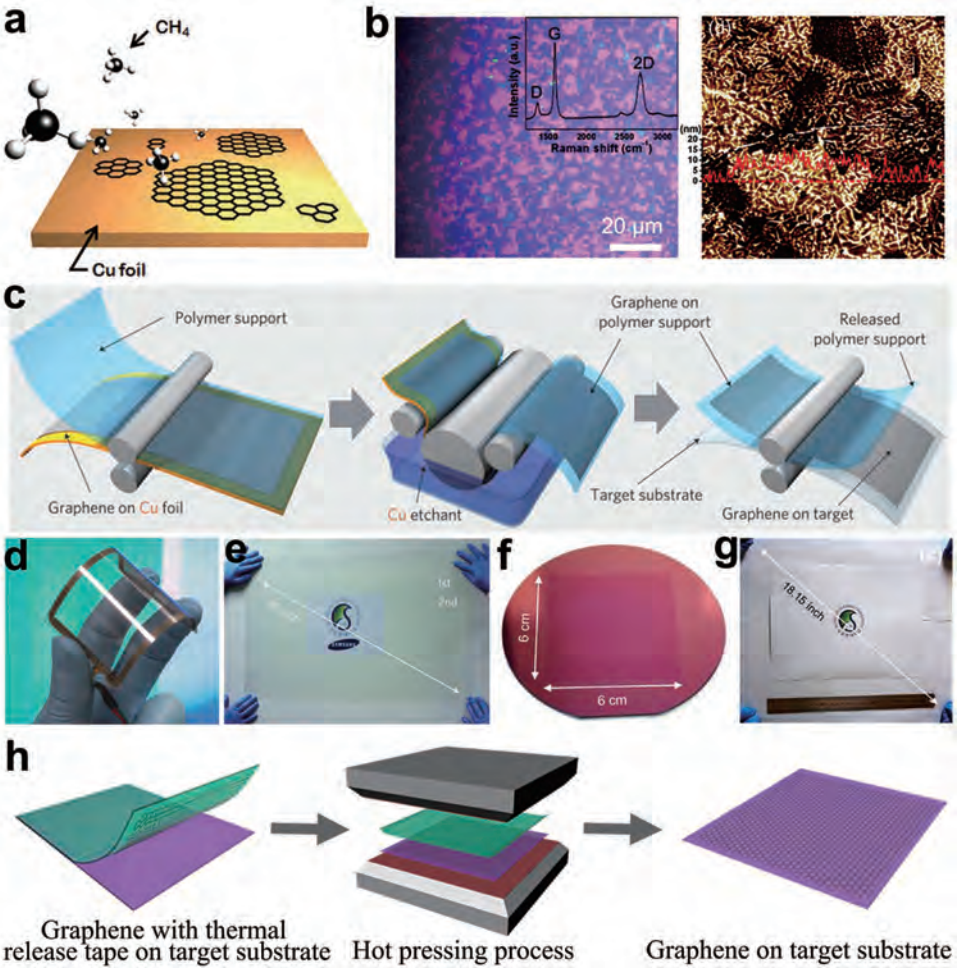

Figure 2. a) Schematic illustration of the graphene synthesis mechanism on metal (Cu) foil. Reproduced with permission.[63] Copyright 2013, American Chemical Society. b) Optical and topography images of CVD-grown graphene. Reproduced with permission.[64] Copyright 2011, American Chemical Society. c) Schematic of the roll-to-roll production of graphene films grown on a Cu foil. d) An assembled graphene/poly(ethylene terephthalate) (PET) touch panel showing outstanding flexibility. e) A transparent ultralarge-area graphene film transferred on a 35 in. PET sheet. (c–e) Reproduced with permission.[74] Copyright 2010, Nature Publishing Group. f) Photograph of a graphene film transferred onto an SiO_2/Si wafer by the hot pressing method. g) Photograph of an 18 in. graphene film transferred on a glass substrate. h) Schematic illustration of graphene transfer by the hot pressing method. (f–h) Reproduced with permission.[75] Copyright 2013, American Chemical Society.

2.2. Solution-Processed Method

Compared with CVD-growth graphene, the solution-processed method provides a feasible approach to produce reproducible and massive graphene films.[76–78] The method includes two main steps: graphite exfoliation in liquid phase and graphene generation by oxidation–reduction process. In this method, hydrosoluble graphene oxide (GO) is produced first by strong acids and oxidants. Subsequently, GO is exfoliated by sonication taking advantage of the interactions formation between the water and oxygenic functional groups. Then, after purification through the ultracentrifugation method, the obtained GO can be reduced to reduced graphene oxide (rGO) via chemical reduction[79] (e.g., hydrazine and sodium borohydride), thermal reduction,[80] or microwave irradiation.[81] However, the oxidation process always suffered with environmental pollution, explosion hazard, and time-consuming reaction to produce large-scale graphene, thus limiting its physical properties and real applications. For the rGO prepared by the solution-processed method, the sheet resistance is up to ≈640 Ω sq^{-1} after thermal annealing at 1000 °C. Recently, a rapid preparation method of single-layer GO in 1 h was developed by Gao and co-workers using a strong oxidant K_2FeO_4 and iron-based green strategy (**Figure 3**a,b).[82] The fast reaction only required ≈15 min intercalation–oxidation process and ≈45 min oxidization–exfoliation process. Meanwhile, it avoided the introduction of contaminative heavy metals and poisonous gases in synthesis process. The ultrafast exfoliation was resulted from the outstanding oxidation abilities of both K_2FeO_4 and the in-situ-generated atomic oxygen. Such a safe, low-cost, high-efficiency, and environmentally friendly approach indicated the feasibility of large-scale production and commercial applications of graphene. Employing the hydrosoluble GO, a continuous fiber (1D) with highly compact and ordered structure, a film (2D) with a well-aligned lamellar structure and good mechanical performance, an aerogel (3D) prepared by a synergistic assembly

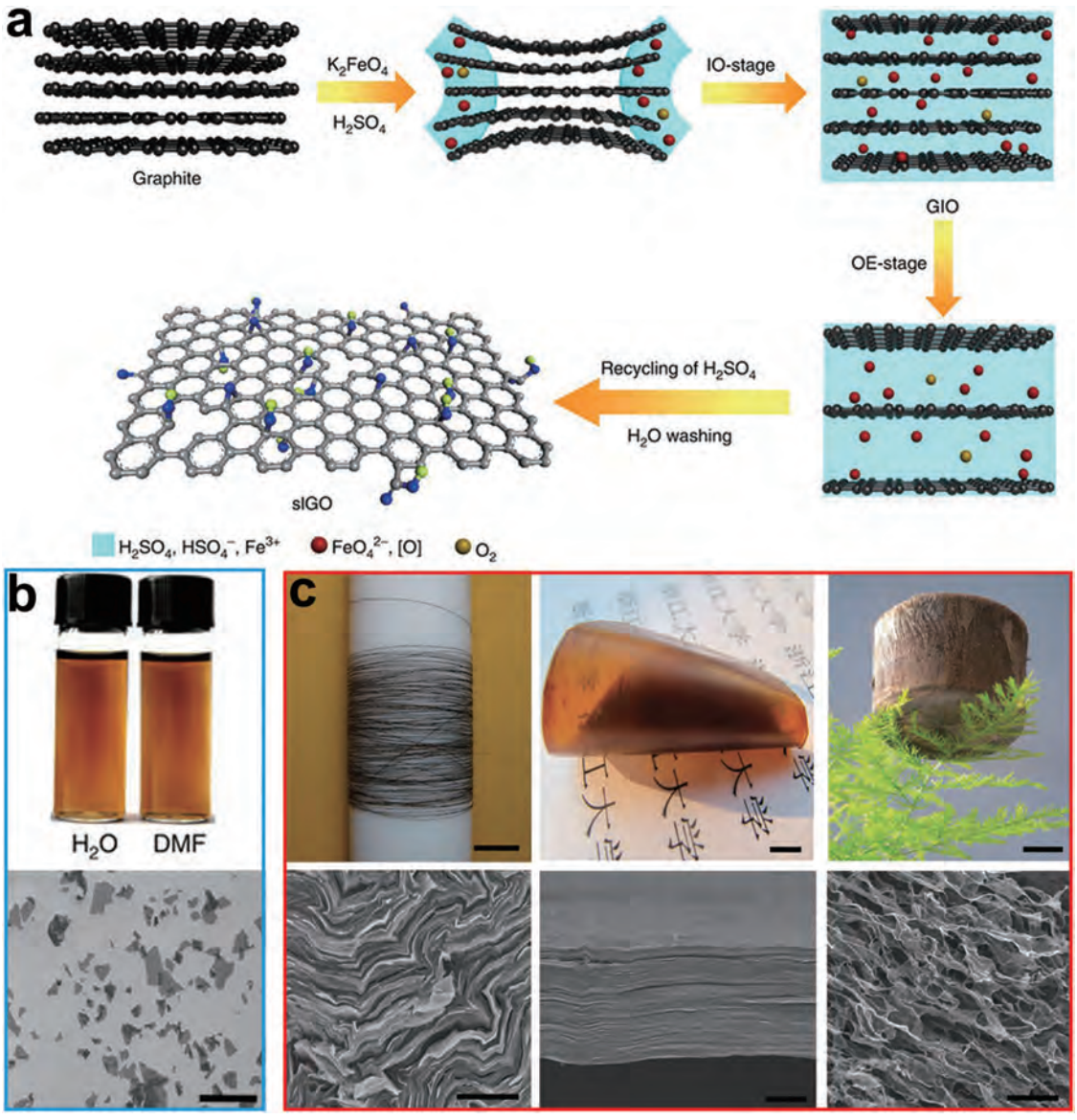

Figure 3. a) Mechanism of GO synthesized with the oxidant of K_2FeO_4. IO is the short name of intercalation-oxidation and OE of oxidation–exfoliation. b) GO solution in H_2O and dimethyl formamide (DMF). c) Macroscopic assembled materials of redissolved GO. From left to right, the images are the long continuous fiber made by wet spun, a film by filtration, ultralight weight GO aerogel and their scanning electron microscopy (SEM) images, respectively. All panels reproduced with permission.[82] Copyright 2010, Nature Publishing Group.

of GO and CNT could be easily fabricated (Figure 3c). Various graphene nanostructures are beneficial to build the graphene-based E-skins with different device structures.

GO is an electrical insulator and must be reduced to make it conductive in most conditions for practical applications.[83] Different from CVD growth, this approach mostly introduces large numbers of oxygenic functional groups (e.g., carboxyl, epoxides, and hydroxyl groups) and defects attached onto the graphene basal plane and edges.[84] The physical properties may be degenerative due to the unavoidable contamination. The obtained rGO mostly possessed an inferior transparency and mechanical properties which were several orders lower than that of pristine graphene. The transparency of graphene is relative to the number of layers and the quality of prepared graphene, due to that the opacity is increasing ≈2.3% with the addition of each graphene layer.[85] A higher annealing temperature will bring a higher transmittance.[86] The quality of rGO is also affected the mechanical properties for the existence of defects and grain boundaries. As reported, the monolayer GO sheet had a lower Young's modulus of 207.6 ± 23.4 GPa, and the GO paper self-assembled from GO sheets was only ≈32 GPa.[87] Interestingly, toward some sensor devices, the functional groups and defects can help reduced graphene to achieve a tunability of chemical and electrical properties than CVD-growth graphene in some special fields.[88–90] Overall, the solution-processed method enables a large-scale production of graphene films at low cost and hold great advantages over assembling flexible E-skin devices. But great efforts should also be focused on promoting the film

properties for the ever-increasing graphene-based electronic devices.

3. Multimodal Sensing of Graphene-Based E-Skins

The excellent characteristics of graphene combined with the productive ability efficiently make graphene a preferred choice for the application of flexible and wearable E-skins. Great progress has been made in the graphene-based E-skins during the last few years.[52,91,92] Except for the active materials to sense external stress (e.g., pressure, strain, and torsion), temperature, and humidity signals, graphene can also be used as electrode materials or enhanced materials to support the signal transmission or improve the sensing property.[93,94] Moreover, the easy assembly of graphene structures such as 1D fiber-like, 2D film, and 3D foam-like can provide a guarantee to serve as flexible tactile sensor of E-skins.[95,96] In this section, we will discuss the types of graphene-based E-skins and their applications.

3.1. Graphene-Based Tactile Sensors

Human skin always receives various stimulations from external stress and results in the pressure, strain, or torsion deformation of skins. Under the stress site, human skin can perceive and distinguish the applied stimulation by sensory nerve ending of epidermis.[5] Bioinspired tactile sensors can realize the similar functions to sense external stimulations such as pressure, strain, and torsion. Graphene as the active sensing material has been widely used in the manufacture of tactile sensors.[97–99] Generally, the sensing mechanisms of graphene-based device prepared by different methods are different. For the CVD–graphene-based strain sensor, it showed an initial reduction in resistance due to the relaxation of pre-existing wrinkles in the graphene film and exhibited a subsequent increase in resistance resulting from the deformation of the hexagonal honeycomb structure of graphene under applied strain–stress.[100] However, CVD–graphene usually exhibits a lower gauge factor owing to the restricted strain-induced structural distortion and a large strain always causes unrecoverable structural damage of CVD–graphene. Therefore, graphene film with a periodical rippled nanostructure was fabricated to endure large strains to achieve a larger relative resistance change.[101] In addition, CVD–graphene could also be used to build 3D composite foam with PDMS to detect bending and stretching deformations by inducing variations in the overlapping contact areas between adjacent graphene layers under external force.[102] For the rGO prepared by the solution-processed method, the contacts between self-assembled graphene sheets contribute predominantly to the integral resistance change. The 3D elastic rGO aerogel with the ordered microstructure showed excellent sensitivity toward pressure deformations. The superiority may be owing to the more effective conductive channel provided by orientated rGO upon external pressure.[103]

To mimic the tactile detection ability for external pressure, strain and torsion just as human skin, tactile sensors need to possess sensory abilities while stimulated by external stress. Generally, tactile sensors are based on the mechanisms including deformation-induced change in resistance, capacitance, and piezoelectricity and triboelectricity as shown in **Figure 4**. The graphene-based tactile sensors with different types of sensing mechanism and their performance are covered below (**Table 1**).

3.1.1. Piezoresistive Tactile Sensors

Owning to the good electrical conductivity and nanoscale flexibility, a weeny stress deformation applied on graphene-based tactile sensor can result in a dramatic change of resistance. The piezoresistive effect makes graphene an ideal sensing component to detect tactile signal in wearable devices. As a common type of tactile sensor, graphene-based piezoresistive tactile sensors own significant superiorities such as broad detected range, low power consumption, easy to device assemble, and signal reading. Owing to these superiorities, piezoresistive tactile sensors have been widely explored and revealed great potential in frontier applications such as wearable E-skins and human–machine interfaces.[112–114] To acquire graphene-based tactile sensors with high performance, various device structures likes 1D fiber-based, 2D planar-based, 3D spongy-based tactile sensors have

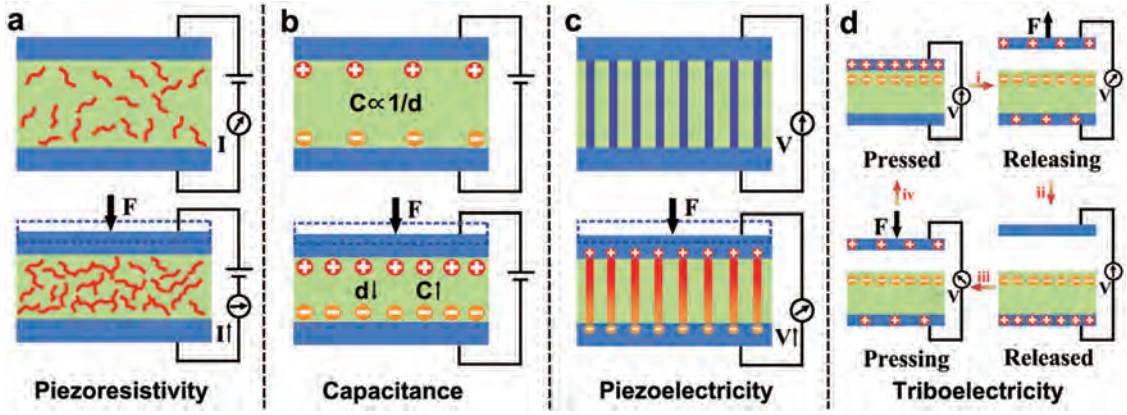

Figure 4. Schematic illustrations for four types of transduction mechanism in a tactile sensor: a) piezoresistivity, b) capacitance, and c) piezoelectricity, d) triboelectricity.

Table 1. Summary for different types of tactile sensors and their performance parameters.

Active materials	Sensing mechanism	Deformation detection	Detected range	Sensitivity/gauge factor	Reference
Wrinkled CVD–graphene	Piezoresistivity	Pressure	100 Pa to 4.5 kPa	6.92 kPa^{-1} (300 Pa < P < 1.5 kPa)	[97]
rGO/PU sponge	Piezoresistivity	Pressure	5 Pa to 10 kPa	0.26 kPa^{-1} (P < 2 kPa)	[104]
rGO/Nano-cellulose films	Piezoresistivity	Strain	0–100%	7.1 (ε = 100%)	[105]
rGO/PDCY fiber	Piezoresistivity	Strain	0–650%	3.7 (ε < 50%)	[106]
Graphene/PS sponge	Capacitance	Pressure	2.3 Pa to 20 kPa	1.04 kPa^{-1} (13 Pa < P < 260 Pa)	[107]
GO foam	Capacitance	Pressure	0.24 Pa to 4 kPa	0.8 kPa^{-1} (P < 1 kPa)	[108]
CVD–graphene/Ag-nanowires' network	Capacitance	Strain	0–200%	22.9	[93]
Ag NWs/rGO/PU composites	Capacitance	Strain	0–60%	0.1	[109]
Interlocked microdome PVDF/rGO	Piezoelectricity	Pressure vibration	0–17.15 kPa	35 mA Pa^{-1} (P < 2.45 kPa)	[110]
$PbTiO_3$ NWs/CVD–graphene	Piezoelectricity	Pressure	0–1.4 kPa	9.4×10^{-3} kPa^{-1}	[111]

been designed over the past several years.[115–118] Generally, the sensing mechanism of piezoresistive tactile sensors is focused on the elastomer composites which acquired by incorporating graphene into polymeric elastomers such as polyurethane (PU), polyvinylidene fluoride (PVDF), polystyrene (PS), and PDMS.

However, the device architecture of the piezoresistive tactile sensor has great effects on the sensing performances. Recently, Chu and co-workers[119] reported a flexible pressure sensor based on GO/rGO hybrid structure with typical piezoresistive effects. The pressure sensor exhibited an ultrafast dynamic detection and frequency-independent resistive sensing behaviors. However, the sensitivity in the low-pressure region is lower compared to that based on composite structures. Therefore, the research on the device structure design has been a hotspot in order to improve the sensing performance of graphene-based tactile sensors.[120,121] For instance, our group[122] reported a planar piezoresistive tactile sensor which was fabricated by wrapping rGO nanosheets on the poly(vinylidenefluoride-*co*-trifluoroethylene) (P(VDF-TrFE)) nanofibers to form a uniform and conductive networks as shown in **Figure 5**a. The sensing mechanism could be explained as that external pressure resulted in a small compression of the conductive film and generated more conducting pathways on the rGO/P(VDF-TrFE) networks, thus leading to a decrease of device resistance. While the applied pressure was removed, contact points are recovered to their original condition and the device resistance increased. The flexible tactile sensor exhibited a high sensitivity of 3.1 kPa^{-1} in very low pressure regime (below 60 Pa) and 15.6 kPa^{-1} in high-pressure regime (above 20 kPa). The sensitive tactile sensor was endowed the abilities to detect ultralight objects like a feather and rice grain as shown in Figure 5b. In addition, the high sensitivity and fast response time enabled it to monitor the wrist pulse and speech recognition in real time, which brought great potential applications in health monitoring and human–machine interaction.

In order to further improve the sensitivity and low detection limit of a tactile sensor, a common strategy is utilizing flexible substrates with microstructures (e.g., micropyramid and microdome arrays on PDMS) for the assembly of tactile sensors.[123] The sensitivity of a tactile sensor with microstructured substrates exhibited several decade times higher than that assembled with planar substrates.[124] The reason can be concluded as that the sharp microstructures on PDMS surface enable the conductive networks with more sufficient contact sites, resulting in a high sensitivity even upon a teeny pressure.

Since the successful realization of 2D graphene film, graphene-based 3D structures such as porous sponge, foam, and aerogels, which can be acted as the structural scaffold, have drawn great attentions for the fabrication of tactile sensors.[125–127] Due to the excellent electrical and mechanical characteristics, graphene possesses unique advantages to extend 2D graphene films into 3D macroscopic architectures with lower brittleness and higher compression resilience ratios. The researches usually employ a self-assembly chemical process to construct 3D rGO architectures, such as the template method with graphene dip-coating and GO freeze-drying methods. To build 3D graphene blocks in macroscopic structures with excellent flexibility and compressive stability, a key factor is the efficient filling of graphene in polymer scaffolds (e.g., PDMS and PU) to form nanostructured conductive sponges. There have been many reports on the fabrication of flexible 3D graphene structures with desired geometry, tunable densities, low resistance, and scalability to mass production.[128,129] However, there is also space to improve the uniformity for the prepared 3D graphene. For example, Ren and co-workers[127] reported a tactile sensor with porous CVD–graphene network combined with PDMS, employing nickel foam as a template and following chemical etching. The tactile sensor had abilities to sense pressure and strain–stress with a wide pressure sensing range (0–1800 kPa) and monitor the human motion such as the walking states, finger bending, and wrist pulse beating in real time. However, the pressure sensitivity is too lower to precisely detect the external stress which has hindered their application in flexible E-skin. To improve the piezoresistive sensitivity, Yu and co-workers[104] designed a novel fractured microstructure in 3D conductive sponges to fabricate a sandwiched tactile sensor as shown in Figure 5c. A random PU fiber network was used to imitate the conductive sponge which owned a fractured microstructure, and then rGO nanosheets were wrapped on it. The sensing mechanism was based on the resistance variations caused by the contact site changes among PU nanofibers during external compression. After a pressure applied on the surface of the sponge, the rGO-wrapped PU nanofibers would contact with each other, thus leading to a large increase in the contact area of the conductive networks. While the pressure

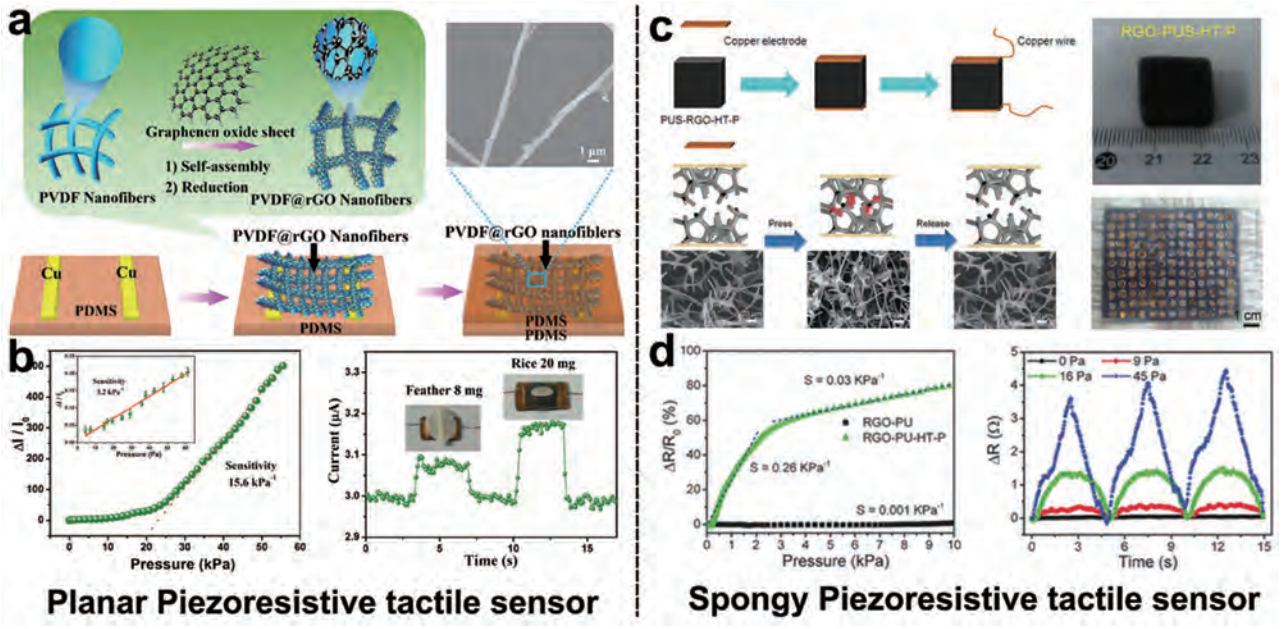

Figure 5. Types of different structures for piezoresistive tactile sensors. a) Schematic illustration of the fabrication and mechanism for a flexible PVDF/rGO-based planar tactile sensor. b) High sensitivity at a broad detected range and the transient response to the loading and unloading of ultralight objects. Panels (a) and (b): Reproduced with permission.[122] Copyright 2016, Elsevier Ltd. c) Schematic illustration of the fabrication and mechanism for an rGO/PU-based spongy tactile sensor. d) Sensitivity for the rGO/PU spongy tactile sensor and multicycle curves of repeated loading and unloading of different pressure values. Panels (c) and (d): Reproduced with permission.[104] Copyright 2013, Wiley-VCH.

removed from the sponge, the deformation of fiber networks would be recovered, resulting in a decrease in the contact area of the networks. Therefore, the pressure sensitivity of the rGO/PU sponge was determined by the variation rate of contact among the PU nanofibers under compressive stress. The rGO/PU tactile sensor with fractured fiber networks possessed an enhanced sensitivity (≈0.26 kPa^{-1}) in the 0–2 kPa pressure regime, which was two orders of magnitude higher than that of the original rGO/PU sponge (Figure 5d). The studies make the 3D spongy graphene architecture a promising candidate for manufacturing low-cost artificial skin. There are many other reports on 3D structure based on other conventional materials such as metal-based aerogels and CNT-based sponges, which still remain many limitations for the practical applications.[130,131] For example, difficulties for the fabrication of metal-based aerogels are still remained due to the lack of appropriate precursor. In addition, it is also complex to control the morphology and design patterned arrays of devices.

Except for the above device structures, a 1D fiber-based tactile sensor is very desirable for E-skin that the design is expected to be flexible, stretchable, durable and lightweight. The use of graphene in assembling fiber-based tactile sensors can improve the mechanical compliance and work range compared with traditional tactile sensors based on metal and semiconductors. Although some studies have been reported on the preparation of graphene-based fiber strain sensors,[132–134] there still exist predicaments which limit the further applications in E-skin. As vital evaluation parameters, the sensitivity to weeny deformation and detected region have significant impacts on the detectability of full-range human activities, ranging from subtle physiological signals (e.g., pulse beat, blood pressure, and respiration) to drastic body motions (e.g., dancing, running, and finger manipulation). In addition, the sensors in most of the reports were only equipped with a single function, that resulting in a restriction for the detection of complex human physical activities. Gao and co-workers[106] developed a facile strategy to fabricate a fiber-based wearable tactile sensor to detect multiple forms of mechanical deformations, including tensile strain, bending, and twisting. A highly stretchable and conductive fiber was designed taking advantage of compression spring and coated uniform rGO around the PU fiber, as shown in **Figure 6**a. The fiber sensor not only exhibited ultrahigh sensitivity (detected limitation of 0.2% strain) to tensile strain deformation and broad detected range (more than 100% strain), but also possessed outstanding bending and torsion sensitive properties under different stimulations (Figure 6b). However, the stretchable tactile sensors based on other conventional active materials such as carbon black, active carbon, and conductive polymers usually cannot simultaneously attain high sensitivity and high stretchability, which may be the results from their intrinsic defects of the surface or interior structure.[135] The high performances of the graphene-based fiber tactile sensor provided great helps to detect full-range human activities, from as subtle as accurate speech recognition and pulse monitoring (Figure 6c,d), to vigorous human movements, such as in real-time monitoring and recording the complex robot motions (Figure 6e).

3.1.2. Capacitive Tactile Sensors

Capacitive sensing mechanism is another important transduction type for flexible tactile sensors. The capacitance (C) of a

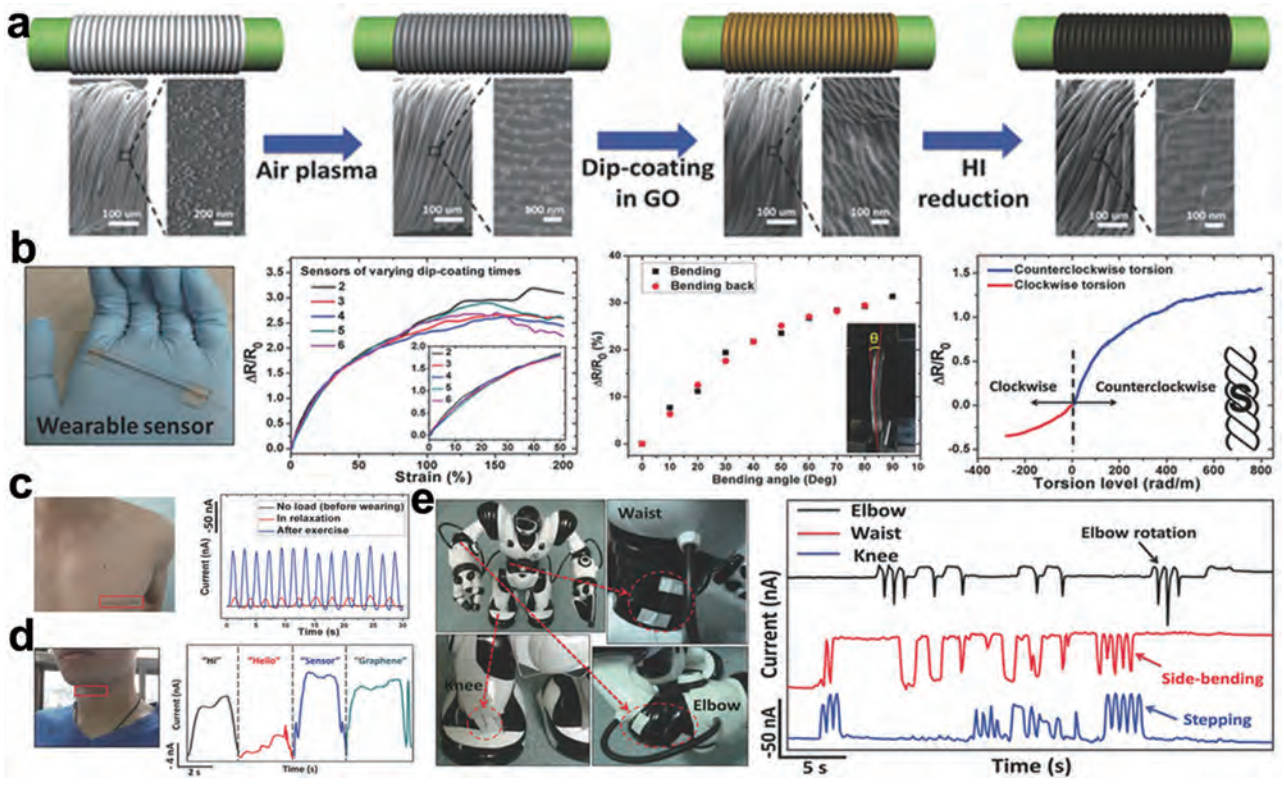

Figure 6. Graphene-based fiber with compression spring architecture. a) Fabrication process of the graphene-based tactile fiber. b) Photograph of the wearable tactile sensor and its sensing ability to detect strain, bending, and torsion deformations. c–e) Applications of the wearable sensors to sense subtle physiological signals and vigorous body movements for human and robotics. Reproduced with permission.[106] Copyright 2015, Wiley-VCH.

parallel plate capacitor can be defined as $C = \varepsilon A/d$, where ε, d, and A are the permittivity, the distance, and the overlapped area between the two parallel plates, respectively. As depicted in Figure 4b, the applied pressure would lead to distance changes of two electrodes and the shear forces would change the A values, thus influencing the capacitance value. Both responses to pressure and strain deformations would result in a signal change of the capacitive tactile sensor. Compared with piezoresistive tactile sensors, the advantages of the capacitive sensors are the much higher sensitivity with low power consumption, faster response speed with less frequency effect,[136,137] whereas the trend of miniaturized devices results in a small sensing capacitance of the capacitive tactile sensor at the magnitude of, approximately, picofaraday, which is more impressionable to the ambient influence due to the low signal-to-noise ratio.[138,139] For example, a pressure sensor based on CNTs/PDMS and an Eco-flex silicone elastomer as a stretchable electrode and a spacer was designed by Bao and co-workers.[140] The tactile sensor presented a relatively small change in the capacitance, thus hindering their application for the detection of tiny pressure. Capacitive tactile sensors with other components and device structures are desired to be developed to improve the sensitivity.

For the capacitive tactile sensor, the compressibility of the dielectric layer is a crucial factor for the device sensitivity.[141,142] Owning to the excellent flexibility, high electrical conductivity, and large surface area, graphene and its conductive elastomers can be used as both the dielectric materials and electrode materials in capacitive tactile sensors. Recently, highly flexible capacitive tactile sensors based on graphene as electrodes or graphene composites with polymers such as PU, PMMA, and PDMS as dielectric layer have been widely reported. Su and co-workers[139] reported a capacitive pressure sensor based on CVD–graphene/PMMA composite film, which could be used as both the dielectric layer and active layer. The high strength of the supporting PMMA layers determined a well-suspended structure of the graphene/PMMA composites. The sensitivity of capacitive pressure sensors which was defined as $s = \Delta C/\Delta P$, was obtained as 15.2 fF kPa^{-1}, almost eight times higher than that of traditional silicon-based materials. However, the low surface capacitance hindered the practical application of graphene-based dielectric. Except for the dielectric layers, graphene has been designed as desired device electrodes to enhance the capacitive sensing property. For example, using the ionic gel matrix as sensing materials and graphene as electrodes, a flexible and transparent capacitive pressure sensor was fabricated by Pan and co-workers.[136] An ultrahigh interfacial capacitance was formed by the electrical double layer, resulting from the accumulation and mutual attraction of electrons on the graphene electrodes and the counter ions from the iontronic film. Noticeably, the capacitive pressure sensor with graphene electrodes showed 40% more sensitively than that with indium tin oxides (ITO) electrodes because of the higher unit area capacitance (approximately in nanofaraday) offered from the interface of graphene ionic.

The design of device structures has a significant impact on the capacitive sensing properties and applications. TS

capacitive tactile sensors have been studied commonly as the touch screens for future wearable devices and E-skins. Effective dimensional changes in elastic dielectrics and stretchable transparent electrodes can enhance the endurance to large strains for stretchable capacitive sensors. However, it is difficult to achieve these simultaneously. Employing Ag NWs/rGO as TS electrodes and PU polymer film as dielectric layer, Lee and coworkers[109] presented a stretch-unresponsive TS capacitive tactile sensor. As shown in **Figure 7**a, the Ag NW/rGO electrodes were embed into the PU planar dielectric layer on PDMS substrates to improve stretchability by a simple selective-patterning process. Due to the low Poisson's ratio of PU dielectric layer compared with that of PDMS substrates, the thickness changes of dielectric layer were minimized and the capacitance changes were prevented while the sensor stretching. The ability was beneficial to the stretch-unresponsive tactile signals. When human finger touched the capacitive tactile sensor, the fringing electric field between the top and bottom electrodes was partially decentralized (Figure 7b), thus leading to a reduced capacitance compared to the no finger touched condition. During the finger touching, the capacitive sensor exhibited an instant response and recovery with a stable capacitance variation of larger than 15% (Figure 7c). The stretchable touch sensors arrays with 5×5 pixels could distinguish the touching point of human finger, which proved a potential application in the capacitive touch screen, whereas the sensing uniformity of the device arrays was a little poor for precisely distinguishing the touching distribution due to the immature fabrication technology. As reported, GO, as a derivative of graphene, behaves like insulators ($1–5 \times 10^{-3}$ S cm^{-1}) and shows a high dielectric permittivity ($\varepsilon \approx 10^4$ within the frequency region of 0.1–70 Hz).[143,144] Various 3D ultralight porous GO sponges with excellent elasticity were assembled as a building block of dielectric layer to fabricate flexible tactile sensors.[107] For example, Sun and coworkers[108] reported a highly sensitive tactile sensor, employing porous GO sponge as dielectric layer and graphene as electrodes by a low-cost fabrication process. The porous structure of the 3D GO sponge dielectric combined with GO skeleton made a good elasticity of the tactile sensor and offered more voids for the response to elastic deformation toward extrinsic pressure. As shown in Figure 7d, when the external pressure applied, the device would be compressed which leads to the air displacement. The decrease of distance (d) between the upper and bottom electrodes would result in an increase of effective dielectric constant, finally the capacitance (C) increased. A high sensitivity of ≈0.8 kPa^{-1}, a fast response time of ≈100 ms, and a very low pressure detection limit of ≈0.24 Pa of the capacitive pressure sensor were demonstrated (Figure 7e). Interestingly, both sensitivity and detected pressure region could be tuned by varying the GO sponge density. To realize pressure distribution with a high spatially resolution, a prototype capacitive pressure sensor arrays of 8×8 pixels were assembled. The sensor arrays provided enough spatial resolution to detect the placement of a strawberry (≈18 g) which generated about 3 kPa for each sensor

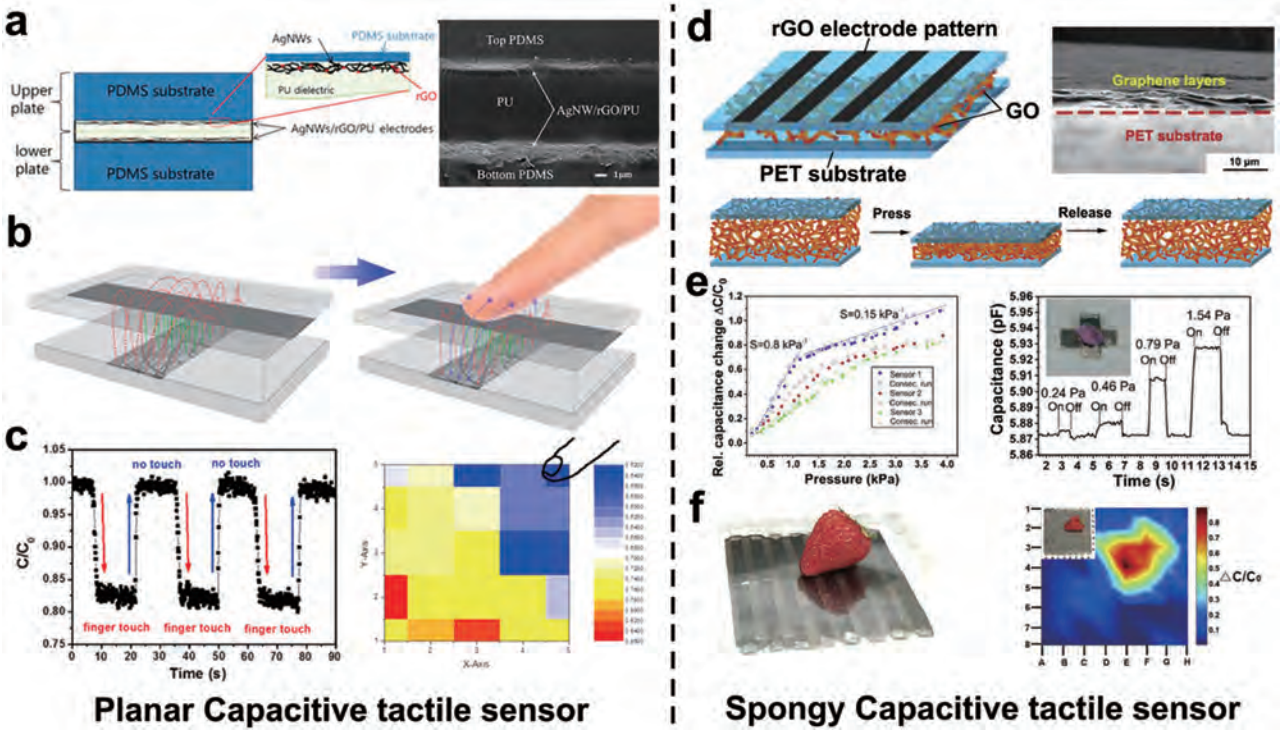

Figure 7. Different device structures for capacitive tactile sensors. a) Structural schematic and cross-sectional FE-SEM image of the AgNW/rGO-based capacitive tactile sensor. b) Tactile sensing mechanism under non-touching and touching states by human fingers. c) Cyclic capacitive response to finger touching over time and the finger-touching detectability of a touch sensor array with 5×5 pixels. Panels (a)–(c): Reproduced with permission.[109] Copyright 2017, American Chemical Society. d) Structural schematic and SEM image of the rGO/GO-based capacitive tactile sensor. e) Pressure sensing properties of the capacitive pressure sensor. f) The ability to detect pressure distribution when a strawberry standing on the tactile sensor arrays with 8×8 pixels. Panels (d)–(f): Reproduced with permission.[108] Copyright 2016, Elsevier Ltd.

(Figure 7f). Hence, the elastic capacitive pressure sensor can pave a way for novel designs of flexible all-carbon electronic devices in human–computer interface applications.

3.1.3. Piezoelectric and Triboelectric Tactile Sensors

Piezoelectricity refers to an effect of generating electrical potentials in response to applied mechanical force for the anisotropic materials due to the occurrence of electrical dipole moments. The piezoelectric property to convert mechanical forces into electrical charges can be assessed quantitatively by piezoelectric coefficient (d_{33}).[145] The piezoelectric sensors have been widely applied to detect the perpendicular vibrations and sliding frictions, due to the high sensitivity and transient sensing abilities. Therefore, effective piezoelectric materials including lead zirconate titanate, ZnO, $PbTiO_3$, and P(VDF-TrFE) have been broadly studied to supersede conventional brittle quartz and ceramics.[146–148] However, there are also many limitations for the piezoelectric tactile sensors such as performance degradation over time, unreliable static response, and susceptibility to temperature which is a confounding factor in the tactile sensing. For example, piezoelectric nanomaterials such as P(VDF-TrFE) nanofibers exhibited non-negligible temperature sensitivity, known as the pyroelectric effect, which may affect the accuracy in reliably detecting absolute stress values without utilizing temperature sensors for compensation.[149]

Graphene has presented significant potential for nano-electromechanical systems. After widely studied for the negative piezoconductive effect of mono-layer graphene,[150] Xing and co-workers[151] reported a positive piezoconductive effect in suspended bilayer and multilayer graphene, resulting from the strain-induced competition between electronic interlayer coupling and intralayer transport. Due to the highly tunable conductivity and excellent mechanical strength, graphene is able to generate a flow-induced voltage with water or polar liquids.[145,152] As reported, it can generate induced potentials in the flow orientation while moving the water droplets with ion-contained over CVD–graphene.[153] However, the underlying substrate creates great influences for the charge interactions between graphene and substrate, and a discrepancy was appeared in generating electric power output. To investigate the function of underlying substrate in the generation of flow-induced potential in graphene, Lin and co-workers[154] designed a type of graphene nanogenerator based on 2D CVD-graphene/PVDF piezoelectric film heterostructures. The nanogenerator can generate electric charges during the flow process of deionized water, tap water, and aqueous NaCl solution from the top end to bottom end of graphene strip (**Figure 8**a). According to piezotronics, the electric charges could be generated at the surface of piezoelectric PVDF film while dropping water onto the graphene surface. Meanwhile, the opposite carriers in graphene and water would be attracted and accumulated at the contact area as shown in Figure 8b and Figure 8c. The incorporation of piezoelectric PVDF substrate under graphene layer led to a flow-induced voltage output of up to 0.1 V with deionized water. The voltage was generated by the retarded screening effect of water for the piezoelectric charges than that of the graphene layer, resulting in a dynamic charging-and-discharging process in graphene. The creation of the flow-induced voltage in graphene provided a novel road for designing graphene-based piezoelectric nanogenerators and self-powered flexible tactile sensors.

However, most of the piezoelectric tactile sensors can only detect the transient signals owing to the instantaneous flow of electrons generated from external load dynamically. In order to measure the static signals, a piezoelectric tactile sensor based on $PbTiO_3$ nanowires and CVD–graphene heterostructures was fabricated.[111] The mechanism was driven by the synergistic effect between strain-induced polarized charges in piezoelectric nanowires and the generated variation of carrier scattering in graphene. The designed tactile sensor was able to measure static pressure signals with an enhanced sensitivity of 9.4×10^{-3} kPa^{-1} and a fast response time of 5–7 ms, which was much faster than other piezoresistive tactile sensors based on graphene.[156]

In addition to piezoelectricity, a new type, named tribotronics, is developed, in which the charges transport in a field-FET is coupled with the extrinsic stimulation through triboelectrification.[157] Owing to the effect of contact electrification, the triboelectric potential can be either positive or negative, which can modulate the ambipolar carrier transport properties for a tribotronic FET. Hence, graphene with ambipolar transport behaviors is an ideal material for the fabrication of triboelectric nanogenerators (TENG). Many studies of flexible graphene triboelectric nanogenerator have been reported.[72,158] For example, a stretchable TENG based on crumpled CVD–graphene structures could harvest mechanical energy under compressive and stretching modes.[147] The TENG device produced a higher output voltage of 9.3 V with 1.5 cm^2 graphene layer, which is proportional to the effective friction areas. The high output voltage was benefited from the crumpled and ripples-like graphene structures, which could create significant amounts of friction and surface charges by the triboelectric effect. Moreover, a graphene tribotronic touch sensor consisted of a CVD–graphene FET and a single-electrode-mode TENG integrated in a coplanar type was demonstrated by Kim and coworkers.[155] Here the triboelectric charges generated from the friction layer of TENG were acted as the gate bias to the graphene FET, which could tune its current transport as shown in Figure 8d. The tribotronic touch sensor was flexible and transparent, and exhibited a high sensitivity of ≈0.02 kPa^{-1}, a detection limit of <1 kPa, a rapid response speed of ≈30 ms, and a high working stability for thousands cycles (Figure 8e,f). The working mechanism could be concluded as the ionic migration as shown in Figures 8g,h. When the PDMS friction layer contacted with a positive touching object, a negative voltage was generated in the ion gel dielectric. The cations migrated to the interface of ITO-ion-gel to screen the negative charges and anions migrated to the interface of graphene-ion-gel in order to accumulate holes in the graphene channel. In addition, the graphene tribotronic device arrays could spatially map various touch stimulation such as gloved and bare fingers touching and the trajectory of a moving ball, thus providing a chance to be applied in E-skins and touch screens. These salient features to harvest ambient mechanical energy allow piezoelectric tactile sensor and triboelectric nanogenerator based on graphene for a variety of potential applications in self-powered wearable electronic devices.

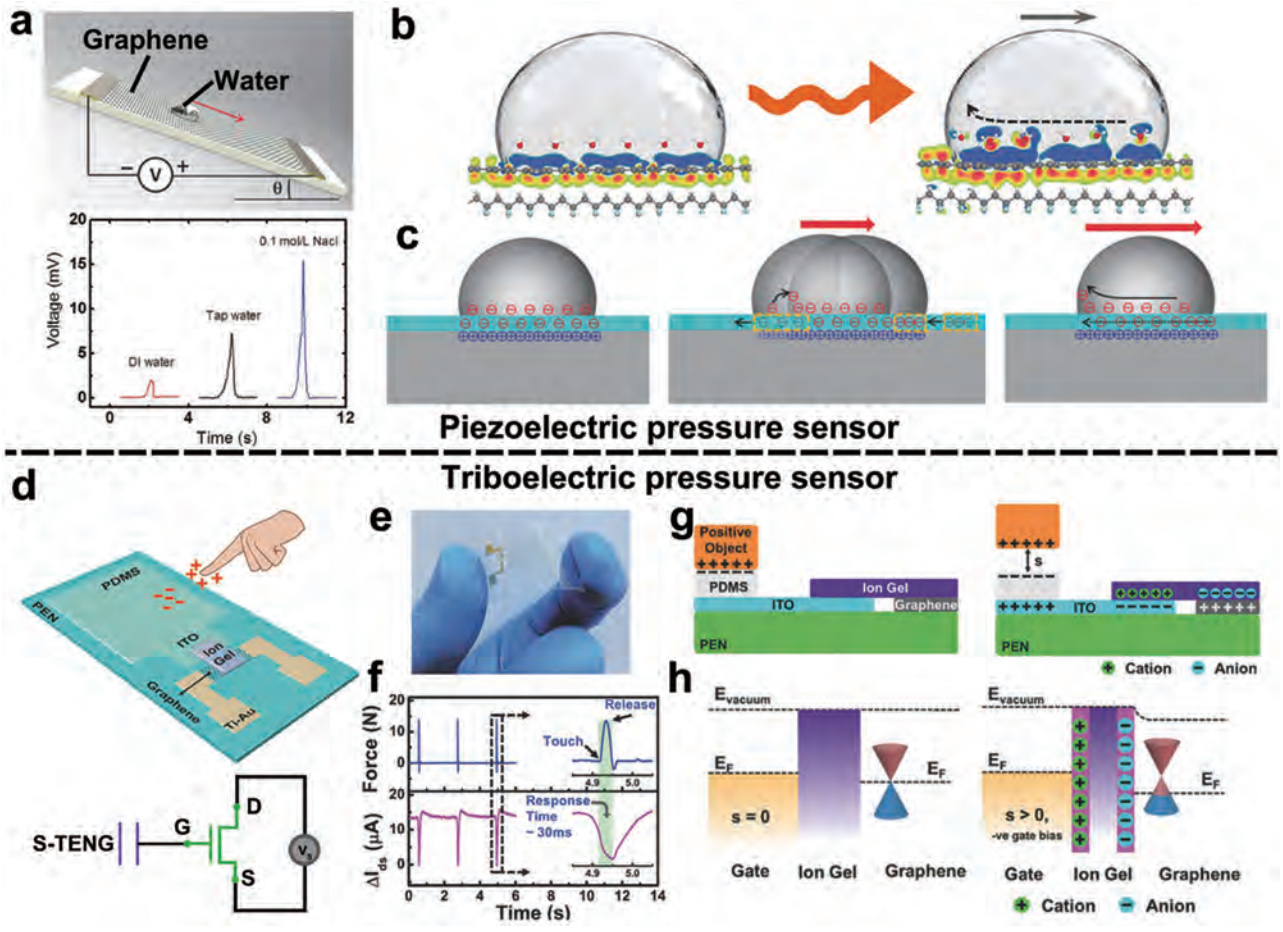

Figure 8. Piezoelectric and triboelectric tactile sensors based on graphene. a) Schematic diagram of the graphene–piezoelectric material heterostructures and typical voltage response to the flow of different types of liquid. b) Illustration of the potential difference induced by moving a pure water droplet from static condition. c) Charge distribution and transfer process during the water flowing process. Panels (a)–(c): Reproduced with permission.[154] Copyright 2016, Wiley-VCH. d) Schematic diagram and equivalent circuit of the graphene-based tribotronic touch sensor. e) Optical image of the flexible and transparent device. f) Current modulation of the triboelectric touch sensor with the touch and release cycles. g) Schematic diagram for the generation and migration of triboelectric charges in the ion gel and graphene while contacted and separated with a more positive external object. h) Energy-band schemata of the gate/ion-gel/graphene interface to depict the doped modes of graphene channel. Panels (d)–(h): Reproduced with permission.[155] Copyright 2016, Wiley-VCH.

3.2. Graphene-Based Temperature Sensors

Temperature-perceiving ability is another significant capability of human skin except for tactile sensing, which helps to preserve the thermal equilibrium between human body and ambient environments. The integration of flexible temperature sensors and tactile sensors makes a meaningful breakthrough for the realization of E-skins and expand their applications in multifunctional electronic devices including personal healthcare and human–machine interactions.[159,160] Temperature-dependent resistance variations can be assessed by virtue of the temperature coefficient of resistance (TCR), which is defined as TCR = $(\Delta R/R)/\Delta T$, where R is the resistance and T is the temperature.

Graphene possesses ultrahigh thermal conductivity (≈5300 W m^{-1} K^{-1}) and thermal emissivity, excellent sensitivity to temperature variation, thus has been widely used in flexible and stretchable temperature sensors.[161] Graphene-based temperature sensors usually show a negative temperature coefficient (NTC) which is distinctively different from other conventional materials.[162] Generally, a multilayer rGO has a larger NTC than CVD–graphene with few layers, because the fluffy structure of rGO can cause more shortening or elongation of volume by heating or cooling. For example, Lee and co-workers reported a temperature-sensitive device based on micropatterned rGO which was inkjet-printed on flexible PET substrate.[163] The as-fabricated rGO thermistors were found to remain a stable operation even under mechanical flexing, and present an NTC that electrical resistance decreased with increasing temperature. A challenge for the flexible temperature sensor in E-skin is the fabrication of stretchable devices which can endure a much higher strain (more than 30%). An effective method to obtain highly stretchable temperature sensors is optimizing the structural engineering of devices such as the construction of electrodes or sensing materials based on serpentine features. For instance, 3D crumpled rGO and Ag nanowires were used as thermal detection channels and electrodes, which were fully embedded in an elastomer matrix

(**Figure 9**a).[164] The device could maintain the temperature-sensing function (≈–2.11% °C^{-1}) even at high stretched states (50% strain) and twisted states due to the mechanical robustness. Moreover, the thermal sensitivity of the rGO thermistors could be effectively tuned by mechanical strain. Compared with traditional rigid thermal sensors, the stretchable temperature sensor presented great potentials to be applied in future stretchable electronics and E-skins. However, the device showed a low TCR, and the temperature-dependent resistance variations were unstable under mechanical deformations upon most occasions. Particularly, rarely all TS temperature sensors based on graphene have been studied for their electrical properties and sensing mechanism under mechanical stimulation. As shown in Figure 9b, Lee and co-workers[165] developed an all-elastomeric TS-gated temperature sensor by a simple spin-coating and lamination process. The temperature-sensing layer was composite materials formed by inserting highly dense rGO nanosheets into an elastomeric PU matrix. The device presented a high stretchability of up to 70% strain, a high TCR of ≈–1.34% °C^{-1}, and a detectable temperature change limit as small as 0.2 °C. Above all, the sensing ability to temperature with the gate structure showed a negligible variation under large mechanical deformation and excellent stability which could endure 10 000 stretching cycles at 30% strain. The TS temperature sensor could be easily attached to objects or human skin as a patch, and monitored the temperature of the object or human skin. Profiting from the ideal flat surface, graphene shows a lower convective heat-transfer coefficient than metals and CNTs, thus resulting in a higher final temperature and a faster heating rate.[166] The temperature sensors based on other thermoelectric materials such as conductive polymer (poly(3-hexyl) thiophene, polyaniline) and semiconductor (V_2O_5 thin films and ZnO nanowires) always show a longer response time and poor mechanical durability.[159,167]

Generally, graphene-based composites exhibit an NTC of resistance to temperature, while most of other conductive composites show a positive temperature coefficient characteristic for the thermal expansion of polymer matrix.[168] To mimic the functions of the sophisticated sensory system in human fingertips, Ko and co-workers[110] reported a human-skin-inspired

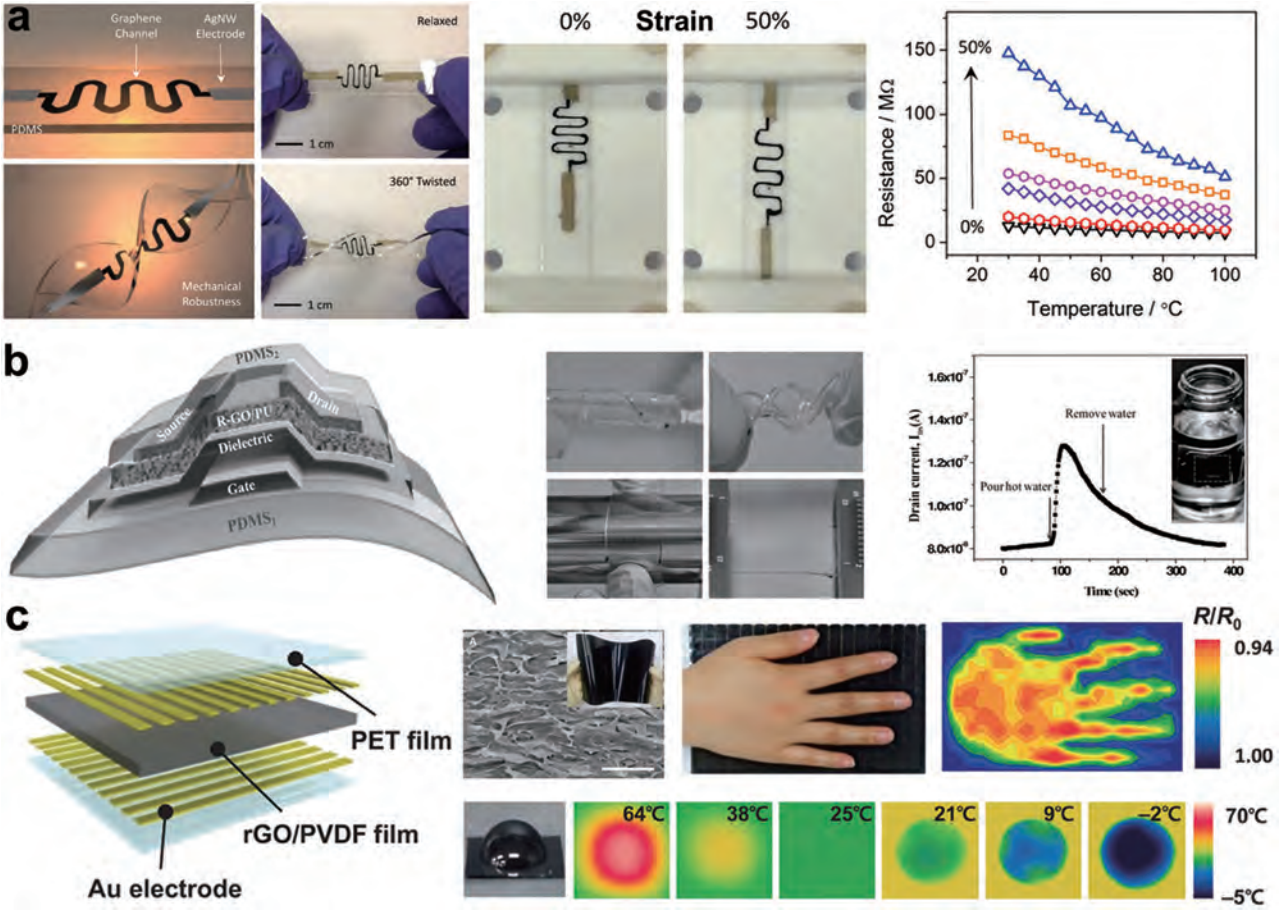

Figure 9. Construction and performance of a flexible graphene temperature sensor. a) Schematic diagram and thermistor performance of the stretchable graphene temperature sensor. Reproduced with permission.[164] Copyright 2015, American Chemical Society. b) Schematic of device structure and stretchable behaviors of the transparent and stretchable gated temperature sensor based on the rGO/PU composite elastomeric conductor. The device can be used to detect the temperature variation of water. Reproduced with permission.[165] Copyright 2015, Wiley-VCH. c) Schematic representation of the flexible rGO/PVDF-based temperature sensor. The device can be used to detect temperature distribution on the human palm and temperature variation of water droplets with different droplet temperatures on the E-skins. Reproduced with permission.[110] Copyright 2015, American Association for the Advancement of Science.

temperature sensor based on the pyroelectric responses of ferroelectric polymer composites consisted of PVDF matrix and rGO sheets (Figure 9c). The temperature sensor showed a typical NTC behavior with a higher TCR of ≈2.93% $°C^{-1}$, which could be ascribed to the variation of contact resistance between the rGO sheets by thermomechanical changes. When human hands were placed on the top of temperature-sensing E-skin arrays integrated with 18 × 12 pixels, the temperature distribution of human could be mapped at the temperature arrays over the whole touching area. Interestingly, the temperature sensor also had the ability to detect the temporal response to continuous changes of temperature. The dynamic resistance variations could be monitored immediately after contact with a water droplet at different temperatures, thus proving a rapid response speed (<0.2 s) and precise monitoring of dynamic and spatial distribution of skin temperature. The scientific and effective designs of the flexible and stretchable graphene-based temperature sensors were enabled to possess outstanding mechanical reliability and high spatial-temporal distinguishability to the ever-changing surroundings, implying that the graphene temperature sensors have potential applications in intelligent robot, artificial E-skin, and human–machine interface.

3.3. Graphene-Based Humidity Sensors

The ability to sense humidity is another important function for human skin by the mechanoreceptors and thermal receptors inserted in the skin, so as to sustain the physiological equilibrium between human body and ambient environments.[169,170] The monitoring of water molecules concentration emanating from human body or surroundings is desired to be useful for personalized healthcare. As for E-skins, the functional mimicry for human humidity sensing is indispensable; thus, flexible humidity sensors that can be wearable or attachable to human skin have been investigated recently.[171,172] To evaluate the performance of the humidity sensor, the sensitivity (s) is defined as $s = \Delta R/(R \cdot \Delta \mathrm{RH})$, where R is the resistance of the humidity sensor and ΔRH is the relative humidity change. At present, many commercial humidity sensors usually use porous ceramics such as Al_2O_3 and SiO_2 as active materials. However, these materials possess inevitable stiff and fragile properties, thus limiting the application in wearable electronics.[173] Although flexible and stretchable polymers always exhibited more linear response than those porous ceramics as the dielectric layer, they may suffer performance degradation at high humidity level for long-term use.[174]

Graphene is a promising candidate of the hygroscopic material to fabricate a humidity sensor owing to its large specific surface area of 2600 $m^2\ g^{-1}$, high chemical stability, and low noise level.[175] In general, the function realization of graphene-based humidity sensors is always attributed to the influence of vapor molecules on charge carrier density of graphene, which result in the variation of resistance of graphene films.[176] For the rGO-based humidity sensor, water molecules can be stably absorbed at the structural defects of rGO surface by hydrogen bonding with oxygenated functional groups covering the defects, thus increasing the resistance of rGO.[177] Humidity can also strongly affect the structures and properties of GO films, because the hydrophilic groups on GO layers make water molecules readily adsorbed via hydrogen bonding.[178] Here, water molecules can act as spacers for the interlayer nanochannels, and humidity can generate distance changes between adjacent GO layers reversibly, thus GO films can be used to build capacitive humidity sensors. Although many humidity sensors based on graphene and chemically modified GO films have been reported recently and exhibit a high sensitivity with a ppb level and fast response speed with a subsecond, they still remain a limited flexibility and stretchability.[179,180] It is urgent to develop TS humidity sensors that can be conformally attached to the human body for the next-generation humidity sensor applications in multifunctional E-skins.

Employing rGO/PU composites as the sensing layer and PEDOT:PSS/PU dispersion as elastomeric conductive electrodes, Lee and co-workers developed a TS humidity sensor on PDMS substrate.[181] As shown in **Figure 10**a,b, the device displayed a high transparency (≈78%) and stretchability (up to 60% strain), a broad detection range (≈10–70% RH), and fast response and release time (3.5 and 7 s, respectively), which was more faster than other humidity sensors based on inorganic oxide such as SnO_2 nanowires.[182] In addition, the high sensitivity ($s \approx 11.88$) could be remained even under a high stretching state of 60% strain and after 10 000 stretching cycles, proving an ultrahigh stability of the TS humidity sensor. The device could also be attached to human fingers or skins to dynamically monitor the humidity levels of ambient surroundings and human skins.

To further improve the sensitivity of graphene-based humidity sensors, novel device structures should be developed. For example, Berry and co-workers[183] reported a 1D filar humidity sensor based on graphene quantum dots (GQDs) as shown in Figure 10c. The GQDs were synthesized via an edge-roughening and cleavage process from graphene nanoribbons (Figure 10d), followed by their self-assembly onto poly(allylamine hydrochloride) (PAH) polymer microfibers to construct a percolating network. The humidity sensor exhibited a higher current modulation and higher sensitivity ($s \approx 43$) by the enhancement of GQDs' network, which had a great improvement than other graphene-based humidity sensors (Figure 10e).[181] The sensing mechanism for the GQD–PAH device is primarily attributed to the change in the tunneling distance between GQDs, that it would affect the tunability in electron-tunneling distances by humidity-induced water transport across the hygroscopic PAH microfibers. Although the flexible graphene-based humidity sensors being high sensitive to humidity have been reported, the devices with high accuracy and good repeatability are still waiting to be developed in order to be applied in wearable E-skins.

4. Potential Applications of Graphene-Based E-Skins

Integrated multifunctional E-skins provide an effective way to realize the potential application in human healthcare, motion monitoring, artificial prosthesis, and human–machine interfaces. Recently, the integration of flexible and stretchable devices with multiple functional sensors has been carried out, thus making a great progress for the functional mimicry

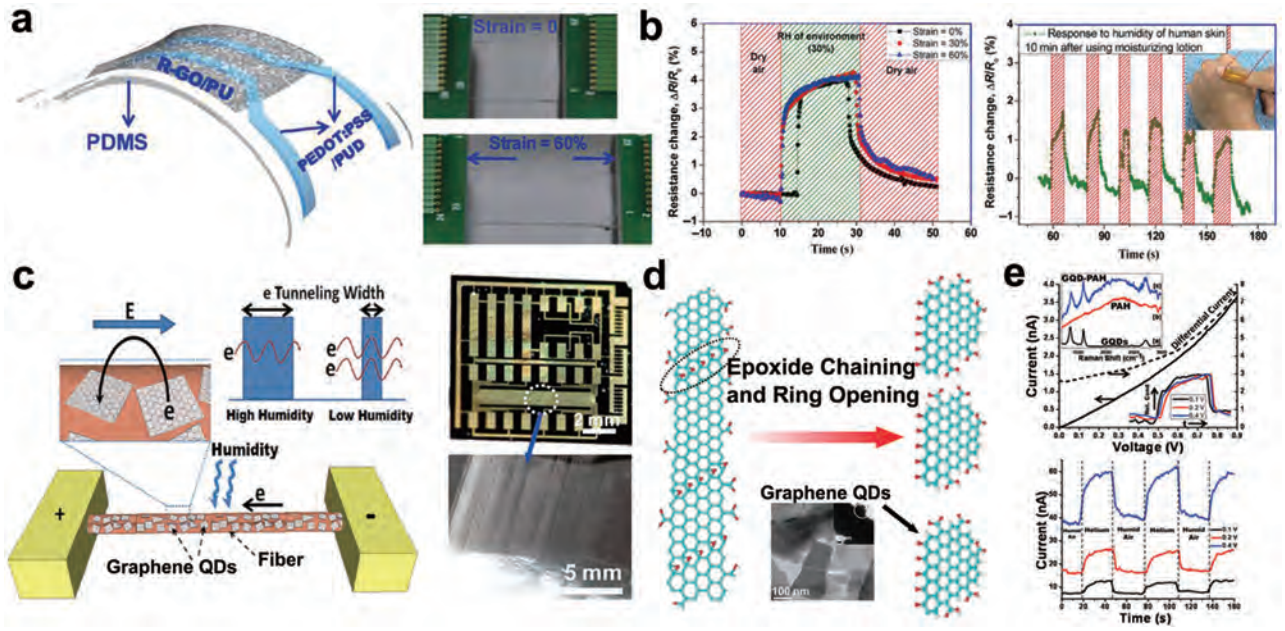

Figure 10. Device structure and performances of graphene humidity sensors. a) Schematic diagram of the transparent and stretchable humidity sensor based on rGO/PU composite sensing layer. b) Resistance variations of the flexible humidity sensor while exposed to different RH concentrations during stretching up to 60%. The device can be used to detect the humidity of human skin on which the moisturizing lotion was applied. (a,b) Reproduced with permission.[181] Copyright 2016, Springer-Verlag. c) Schematic of the sensor's construction and work mechanism for the graphene quantum dot (QD)-based humidity sensor. d) Underlying mechanism to depict the conversion of graphene nanoribbons to graphene QDs. e) Sensing performance of the humidity sensor at room temperature with different operating voltage. (c–e) Reproduced with permission.[183] Copyright 2013, American Chemical Society.

of human skins.[184–187] In this section, we review the recent potential applications achieved in E-skins based on graphene.

4.1. Multifunctional Epidermal Electronics for Biomimetic Human Skins

Many groups have reported flexible graphene-based E-skins with monomodal function such as tactile sensing and temperature sensing in a single device.[188,189] However, it requires a multiple functional integration of graphene-based E-skins, in order to simultaneously perceive and distinguish different stimulations such as static and dynamic tactile, temperature, and humidity for the real realization of biomimetic E-skins. As we know, various sensory receptors and distinctive fingerprint microstructures on human skin enable the perception of ambient temperature, touch, and surface texture. Inspired by the sophisticated structures and functions in human skin, Ko and co-workers[110] developed a multimodal E-skin based on flexible and microstructured ferroelectric films (PVDF/rGO) in order to detect and differentiate multiple spatiotemporal stimulations (**Figure 11**a). Employing the piezoelectric and pyroelectric responses of PVDF/rGO film, the bioinspired E-skins could monitor static and dynamic touch and temperature. The parallel ridge-like elastomeric pattern was used to mimic fingerprint patterns on the surface of E-skins. The microstructures endowed the E-skin abilities to perceive various surface textures with different topological patterns, roughness, and hardness (Figure 11b). The discrimination of various surface textures for graphene-based E-skins has enriched the multifunctional perception and promoted the actual realization of E-skins.

Temperature sensing and elasticity of devices are important parameters for monitoring ambient surrounds and tactile behavior. However, highly stretchable multifunctional sensing is difficult to be achieved for E-skins. The reported devices always showed a low responsivity to temperature and a limited elasticity due to the nonstretchability of internal channel, electrode, or connector.[190] To mimic the simultaneous detection of temperature and strain as human skin, a TS-integrated platform of temperature and strain sensors was assembled in a vertically integrated strategy as shown in Figure 11c.[165] The integrated device with both sensors could be easily attached on a human arm to monitor the temperature variations and muscle movements during human activities such as the motions of drinking hot water and human workout. As shown in Figure 11d, the integrated devices exhibited a high-resolution temperature distribution for the recognition of human activity and achieved a real-time monitoring of human temperature and muscle movement. The TS multifunctional platform showed great potential for applications to wearable epidermal electronics.

In addition to the multiple stimuli sensing for E-skins, a low-cost and facile fabrication procedure is also vital to develop rational sensor architecture based on graphene and its derivatives. As displayed in Figure 11e, Cho and co-workers[34] reported a TS all-graphene multifunctional E-skin sensor matrix which could perceive pressure, temperature, and humidity simultaneously. These three types of sensors based on GO and rGO were handily integrated into a layer-by-layer geometry through a simple lamination process, which could retransmit independent electrical signals. To capture human action stimuli, a TS E-skin sensor matrix with 6 × 6 pixels was fabricated as shown in Figure 11f. When fingers were pressed

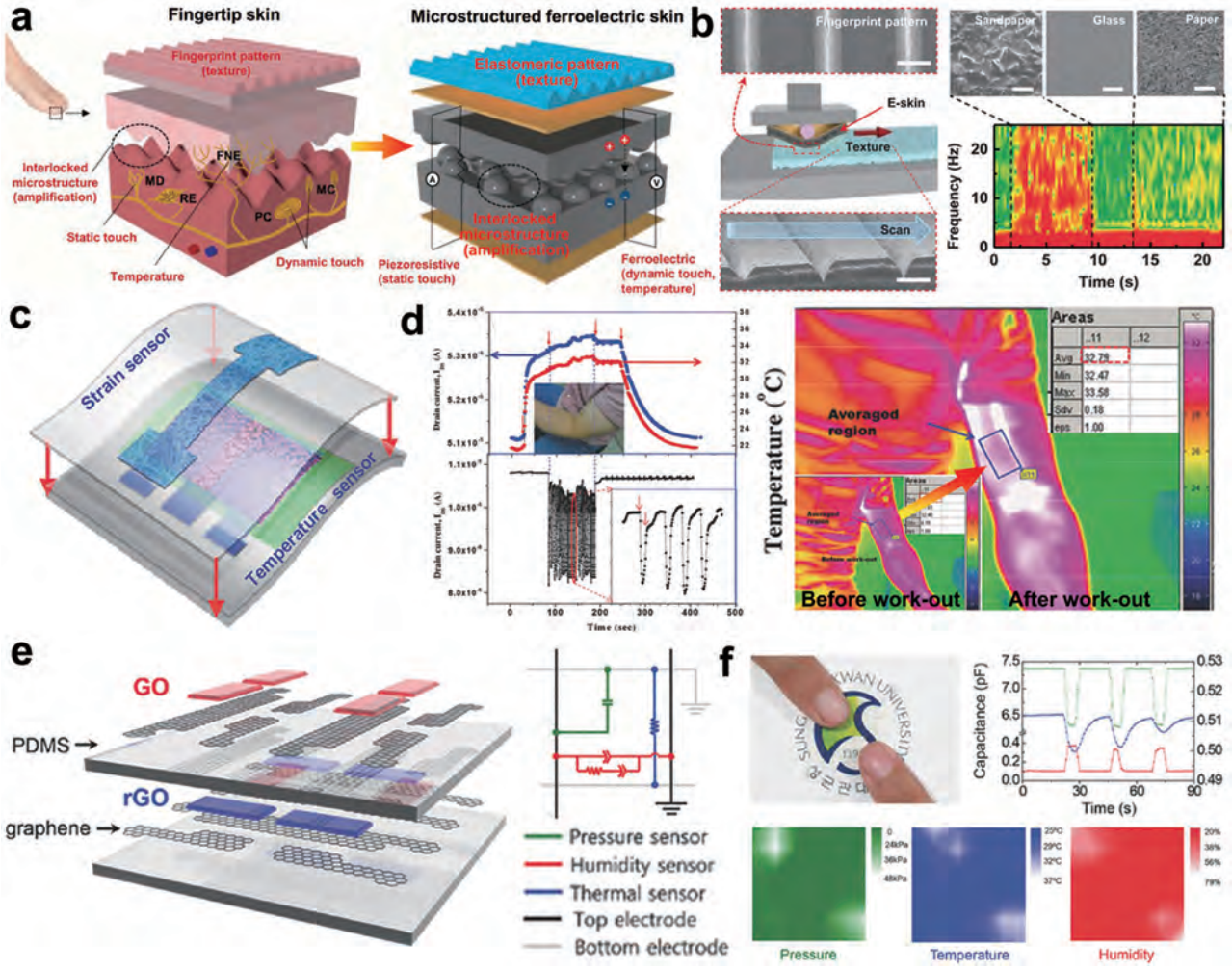

Figure 11. Multifunctional epidermal electronics for biomimetic human skins. a) Human-skin-inspired multifunctional E-skins for the static and dynamic detection of texture, pressure, and temperature. b) Piezoelectric E-skins with fingerprint-like patterns for perception of texture with different roughness. (a,b) Reproduced with permission.[110] Copyright 2015, American Association for the Advancement of Science. c) TS-integrated E-skins with temperature and strain sensors. d) The ability to sense temperature change and muscle movement during human workout. (c,d) Reproduced with permission.[165] Copyright 2015, Wiley-VCH. e) Schematic diagram of the multimodal E-skins which could sense pressure, temperature, and humidity simultaneously. f) The ability of the E-skin to sense three different stimulations while fingers pressed. (e,f) Reproduced with permission.[34] Copyright 2016, Wiley-VCH.

on the sensor arrays, variations of pressure, temperature, and humidity could be monitored simultaneously, demonstrating the multimodal sensing capacities for the graphene-based E-skins. Furthermore, it is necessary to integrate such abilities for graphene-based E-skins as biocompatibility, biodegradability, and conformability with flexible and stretchable sensors to monitor the multiple environmental parameters of human skins and organs.

A great challenge for the multifunctional E-skins is the ability to distinguish among diverse sensing signals simultaneously such as mechanical stimuli, temperature, and humidity from the complex external environment. Due to the influences between the target sensing signals and other external stimuli, attempts have been made to improve the specificity of multifunctional E-skins. To date, most of the integrated devices are employing various discrete sensing elements which are coupling electrically, corresponding to each sensing function.[34,186] This method enables the signal transduction and signal readout mechanisms that can be designed independently to distinguish target signals. For example, capacitive tactile sensors and thermal-resistive temperature sensors can be integrated together without mutual signal interferences. Another approach is to choose different materials as gate dielectrics and channel of FET, which are able to respond to pressure and temperature simultaneously, but in a disproportionate manner.[191] The sensing signal can be distinguished by analyzing the change in the amplitude and offset values of the drain current with AC gate biasing. In addition, sensing signals originating from mechanical disturbance can be minimized at the level of functional sensor via designing compensating circuits and referential devices to calibrate the output signals. However, the mentioned methods have some limitations due to the complex fabrication process and structural designs, thus resulting in inaccurate signal output. Profound studies should also be made to increase specificity for multifunctional E-skins in practical applications.

4.2. Health and Motion Monitoring

Nowadays, the developed E-skins not only have the ability to perceive external stimuli for the mimicry of human skin, but also possess the abilities that human skins do not have, such as the monitoring of human blood pressure, heart beating, and respiration rate.[192–195] These special abilities to detect human vital signs can help to establish an individual system for health protection and remind users or medical professionals of abnormal health conditions, which have broadened the potential applications in individual healthcare and medical diagnostics.

The sensitivity and detection region determine the primary ability of the tactile sensors from monitoring physiological signals as subtle as heart rate and sound vibration to body motions as vigorous as finger action and wrist movements. The recent reports about graphene-based tactile sensors have realized the full-range detection of human activities.[10,196] To capture subtle physiological signals, high sensitivity and detectability in low-pressure region are necessary for the reliable detection of pulse pressure in various locations on human body such as wrist and neck. The most common location for pulse diagnosis is the radial artery, which contains an ascending limb and a descending limb. Different from an electrocardiogram which displays the bioelectrical information in human body, the pulse waves containing three typical pulse peaks are generated from the pressure fluctuation in radial artery.[197] As exhibited in **Figure 12**a, Zhu and co-workers[198] designed a skin-like pulse wave monitoring device based on CVD–graphene strain sensors to acquire noninvasive and real-time detection of cardiovascular parameters. The CVD–graphene-based tactile sensor was easily used and wearing comfort, which was close knit onto the human skin. It can precisely detect and distinguish the pulse waveforms with different ages, pre- and postexercise (Figure 12b). In view of pulse wave originates from the cardiovascular activity, the cardiac contractility and ejection fraction, peripheral resistance and artery compliance, and other vital physiological parameters can be qualitatively analyzed according to the obtained pulse waves, thus providing an inference for the evaluation of health conditions.[201]

The sound detection of E-skins is another exigent function for the deaf-mute people to understand what others say and how they express themselves in a way of electronics. As reported, most of the sound detectors based on graphene are based on the piezoresistive effect that sensing sound through monitoring the movement of throat muscles,[41,202] whereas the piezoresistive-type sound detectors are hard to emit Joule heating into the air as sound sources. To develop an easy-to-use sound detector is urgent which can precisely transform the sound with inapprehensible meaning into understandable sound in languages for the specific people. The requirements that are the abilities to detect and generate sound simultaneously though the common detectors and sound sources are mostly isolated from each other and are noncontinuous within the human audibility range. Employing the direct laser writing, Ren and co-workers[199] designed a wearable artificial throat based on laser-induced graphene (LIG) on polyimide substrate, which could detect and emit sounds simultaneously (Figure 12c). Different from piezoresistive acoustic transducers, the LIG artificial throat worked taking advantage of its piezoelectric effect and inverse piezoelectric effect. The high thermal conductivity and low heat capacity of LIG made it a candidate for the thermoacoustic sound source, and the porous structure endowed a high sensitivity and low limit detection for the weak sound vibrations. The artificial throat could emit a wide-band sound with frequencies between 100 Hz and 40 kHz as a sound source and response toward various sounds and throat vibration modes as a sound detector (Figure 12d,e). More importantly, the intelligent artificial throat had the capability to recognize different intensities and volumes of hum, cough, scream, and to recognize the pronounced words and sentences. Profiting from the ability to convert the unclear vibrations into controllable sounds, the artificial throat paved a way to the specific phonation recognition and speech rehabilitation training for the handicapped.

Monitoring the motion signals of human body has been deemed as an effective method to assess and supervise human kinematic state. In vigorous motion sensing, the E-skin can be fixed onto the knuckle and knee of human body to detect the finger movements and limbs activities.[40,203] The requirements for the tactile sensor are a large detected region for pressure or strain and a high sensitivity. However, traditional tactile sensors based on metal nanowires and semiconductors owned limited stretchability and sensitivity, thus are unsuitable to be used to monitor vigorous motions.[204] Therefore, it is essential to develop highly sensitive, stretchable, and wearable tactile sensors for monitoring human motions. Combined with piezoelectric nanogenerators and coplanar-gated graphene transistors, Cho and co-workers[200] designed an active matrix strain sensor array as shown in Figure 12f. Under continuously applied tension and compression, the integrated devices could maintain stable output signals with a high sensitivity (GF, ≈389) and excellent durability (up to 3000 bending cycles) as shown in Figure 12g. The conformal device could be attached on the hand of human wrist to monitor consecutive hand movements by capturing the current outputs (Figure 12h). Some other reports about graphene-based E-skins have also been demonstrated how to determine the capability to record and discriminate various other motions including knee flexing/extending, walking, jogging, jumping, and running, depending on the obviously differentiable patterns of recorded curves.[106,205] The excellent behaviors for the monitoring of human physiological signals and physical motions provide a tremendous potential for smart wearable devices to achieve health monitoring and motion detection.

4.3. Human–Machine Interaction

Human–machine interaction has attracted much more attentions for the wearable intelligent system because of the wide applications in bionics, robotics, and personal mobile electronics. As human skin shows a crucial role in shaping our interactions with the ambient surrounds, E-skin devices hold far-reaching enlightenments for advanced prosthetics and robotics to mimic the behaviors of human skin.[56] For instance, the development of artificial skins or prosthetic hands with human-like sensory abilities and steerable functions is greatly

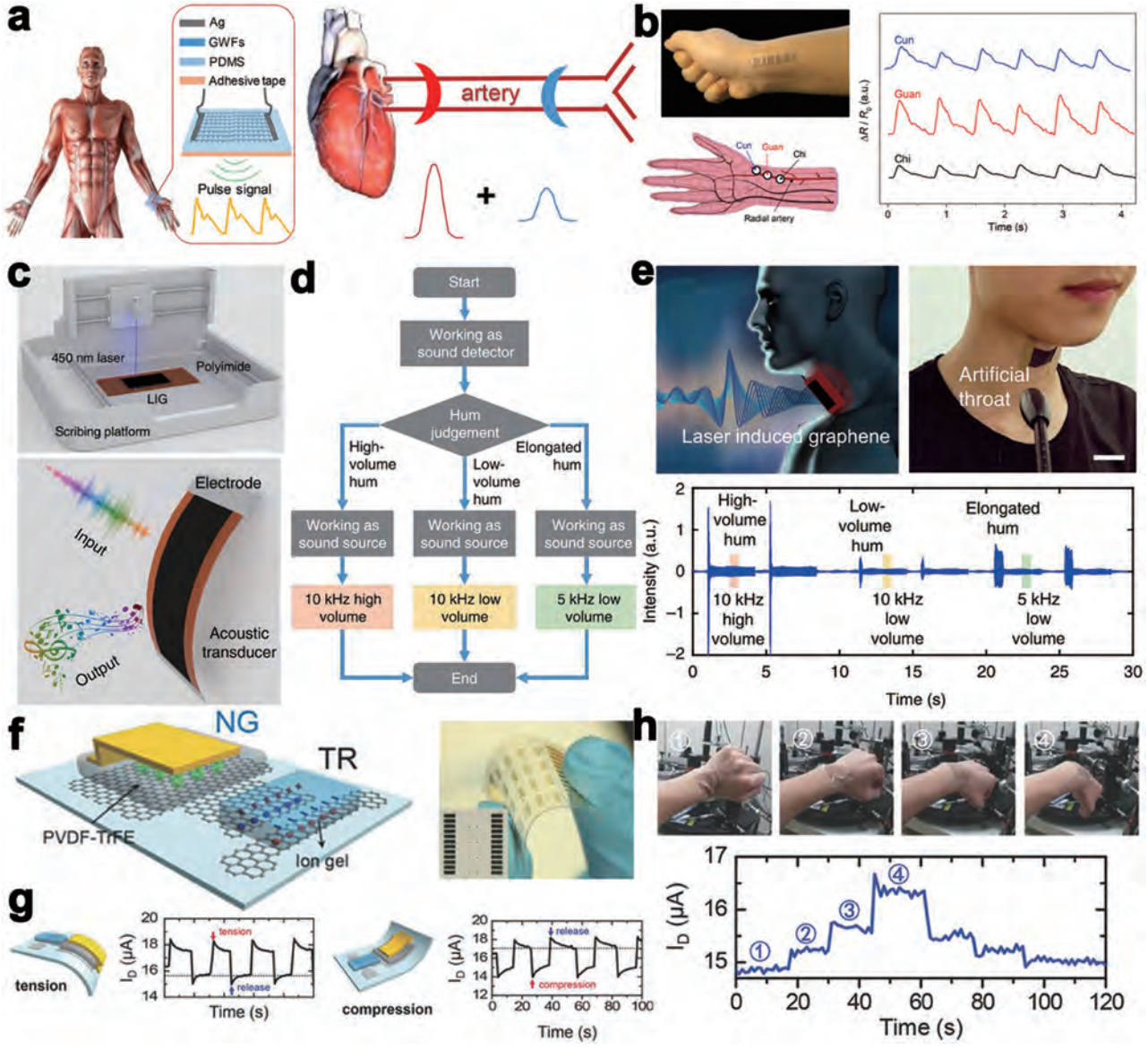

Figure 12. Health and motion monitoring for graphene-based E-skins. a) The device structure of E-skins to monitor epidermal pulse wave. b) The ability to sense pulse on different positions of human wrist. (a,b) Reproduced with permission.[198] Copyright 2017, American Chemical Society. c) The structure of the laser-induced graphene artificial throat and the ability to generate sound and detect sound in a single device. d) The working procedure of the artificial throat. e) The ability of the artificial throat to detect high volume, low volume, and elongated tone hum, and convert them into high-volume 10 kHz, low-volume 10 kHz, and low-volume 5 kHz sound, respectively. (c–e) Reproduced with permission.[199] Copyright 2017, Nature Publishing Group. f) The device structure and active matrix of the flexible strain sensor based on the piezopotential-powered graphene transistors. g) The ability of the strain sensor to sense tensile and compression strains. h) The ability to monitor movement of human hand by the conformal piezopotential-gated strain sensor on PDMS substrate. (f–h) Reproduced with permission.[200] Copyright 2015, Wiley-VCH.

significant for the disabled or intelligent robots that require substitutional prosthetics.[44,206] The mechanical pliability for the electronic devices is required to achieve devices with interactive human–machine interface. When contacted with human skins directly, it can weaken the discomfort and sense different types of free-form deformations during human body motions. Many studies about the graphene-based electronic devices have been reported for the applications of human–machine interaction such as data glove, manipulator, and interactive human–machine interface.[55,207]

Wearable data gloves have attracted much more attentions due to their capacities to systematically monitor the finger movements of human or robots and recognize the gestures in real time.[54,208–210] To assemble high-performance wearable electronic glove, high strain sensing capabilities, and conformal to finger joints are required. For example, Park et al.[134] developed a novel graphene strain sensors based on stretchable yarns by a simple layer-by-layer assembly process. The wearable sensors showed an excellent stretchability (>150% strain) and a wide detection region, thus enabling to easily record and identify the movements

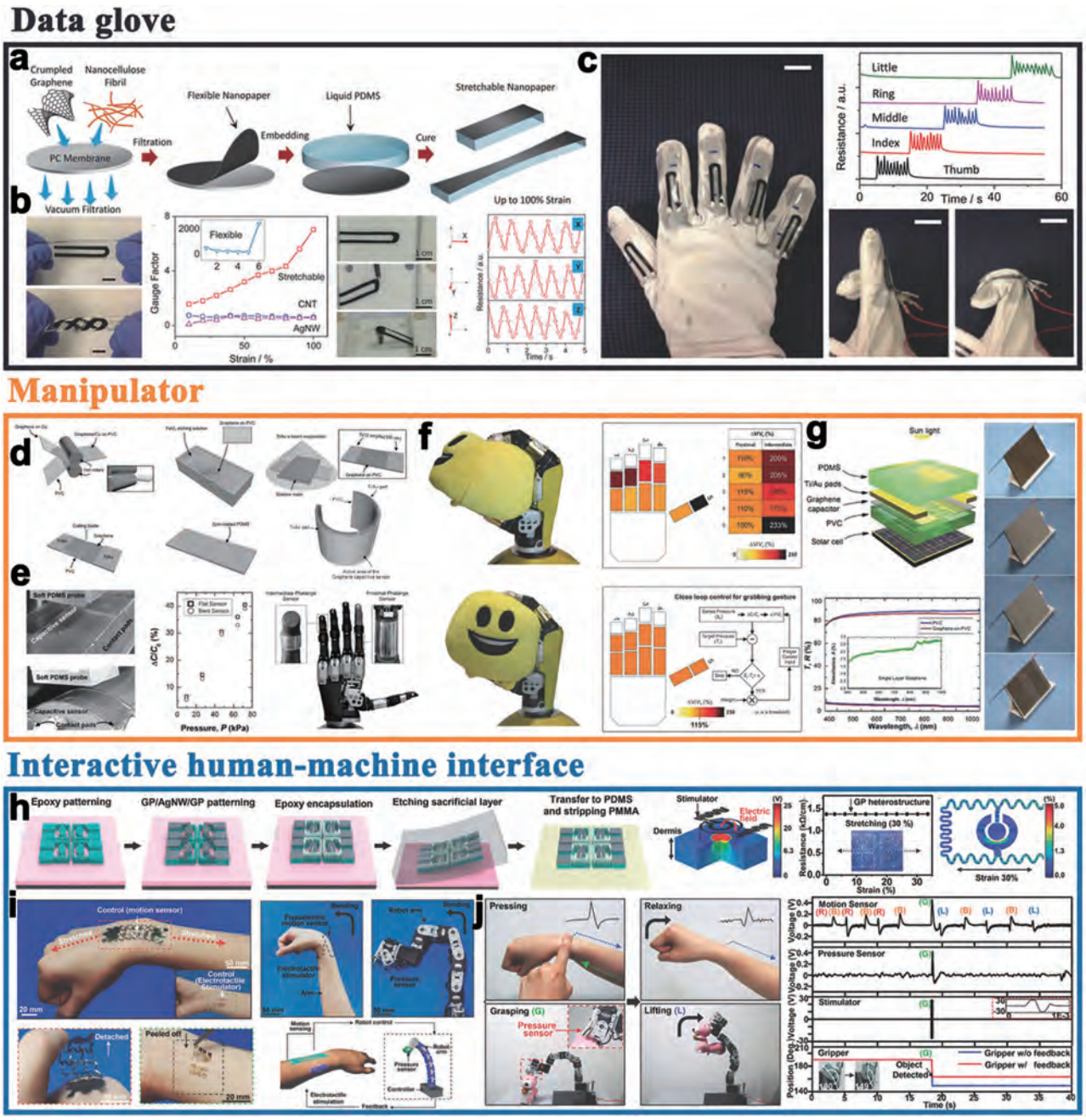

Figure 13. Application in human–machine interface for graphene-based E-skins. a) Schematic illustrations on how to fabricate stretchable graphene nanopapers. b) The excellent stretchable performance of the nanopapers and the ability to response strain deformations in three directions. c) Data glove with five implanted stretchable sensors to detect movement of fingers. Panels (a)–(c): Reproduced with permission.[105] Copyright 2013, Wiley-VCH. d) Schematic illustrations to fabricate graphene-based flexible capacitive touch sensors. e) The ability to detect the capacitance changes while the sensors under bending state and the touch sensors were integrated on an artificial limb to be acted as tactile E-skins. f) Dynamic monitoring of the graphene touch sensor during grabbing a soft object. g) Energy autonomy of the E-skin realized by heterogeneously integrating of graphene transparent touch sensors atop a solar cell. Panels (d)–(g): Reproduced with permission.[211] Copyright 2017, Wiley-VCH. h) Schematic illustrations on how to fabricate the transparent electrotactile stimulator and the ability to sense applied strain. i) The electrotactile stimulator that could be attached on human skins and its ability to control the robot arm by the human motion. j) The pressing and relaxing of human wrist could result in the robot arm to realize the action of grasping and lifting, and their voltage signals detected by the graphene-based tactile stimulator. Panels (h)–(j): Reproduced with permission.[55] Copyright 2014, Wiley-VCH.

of human fingers while the strain sensors were implanted in a glove. In addition, Lee and co-workers[105] designed a piezoresistive strain sensor based on rGO and nanocellulose with a high stretchability (up to 100%). As shown in **Figure 13**a, the stretchable nanopapers based on crumpled rGO and nanocellulose fibril were fabricated and then embedded in the elastomer

matrix. Except for the excellent stretchability, the nanopapers sensors were capable of all-directional sensing, which allowed the efficient detection of diverse types of forces beyond uniaxial strain (Figure 13b). An electronic glove was assembled by five independent sensors implanted in a feather glove to monitor the movements of fingers such as bending and stretching as displayed in Figure 13c. The electronic glove revealed a vital branch of intelligent monitor devices and could be used for fine-motion manipulation in future advanced robotics and virtual reality.

Another potential application of the tactile E-skin is in providing virtual haptic perception to amputees or robots. Dahiya and co-workers[211] developed a transparent capacitive tactile sensor based on single-layer graphene, which was grown by the CVD method and transferred on flexible PVC substrate (Figure 13d). The hot lamination transfer procedure made a good conformal contact between graphene and substrate, resulting in the sensor architecture more robust and steady even under bending state (Figure 13e). The capacitive response of the tactile sensor showed a wide detected pressure region from 9.8 to 72.1 kPa and rapid sensitive speed, which are critical features for further integration with an i-Limb to performing a "Grabbing" test. As presented in Figure 13f, the integrated manipulator could grab soft objects in a controlled way using the touch feedback, demonstrating a great potential application in robotics. Moreover, owing to the high transparency and low power consumption, the tactile sensors could be integrated with a solar cell in the back plane to establish an energy-autonomous tactile skin. As exhibited in Figure 13g, the power–voltage performance was not influenced during touching the covered sensors due to the special transparent behaviors. The novel concept showed a practical prospect toward flexible energy-autonomous E-skins by harvesting natural light energy to drive sensor–transducer-integrated circuits or a robotic manipulator.

In addition, Kim and co-workers[55] designed a TS interactive human–machine interface system consisted of wearable electrotactile stimulators and motion sensors. The stimulator could be transferred onto human skin and exhibited stable performance even after it was stretched by more than ≈30% (Figure 13h). The motion sensor based on patterned graphene heterostructures was assembled via implanting a piezoelectric pressure sensor on the gripper. The close-loop system, as shown in Figure 13I, endowed the motion sensor the ability to monitor human motion in real time and transform information into corresponding signals to control the robot. Conformal integration of the ultrathin and stretchable devices with human skin reduced artifact signals and improved the precision of machine control. Figure 13j displayed the capability of synchronized motion for a robot to be controlled by a human wearer such as manipulating the robot arm to exhibit bending or grasping and lifting motions by controlling corresponding motions of a human. The interactive human–machine interface system presented unparalleled wearability and allowed for sophisticated interactive robot manipulation.

4.4. Spatial Tactile Mapping by Large-Area Integrated E-Skin Arrays

To achieve fully biomimetic E-skins with a high spatiotemporal resolution, high-density sensor arrays with multifunctions are required for E-skins to cover an adequately large area. However, the size reduction leads to an amplitude decline of analog signals such as current signal or capacitance signal, along with the increase in density of sensors and interconnect lines, which engendered increased interference with each other.[212,213] To settle the perplexity, a transistor can be applied to integrate with each sensor to accomplish local signal conversion and amplification. Besides, it can also expedite the development of multiplexing technology during building an active matrix, thus efficiently decreasing the number of required interconnect lines.[214]

Recently, Park and co-workers[196] designed an unconventional strategy to fabricate fully integrated active matrix arrays formed by two folding panels, employing CVD–graphene-based pressure transistors with air dielectric layers (**Figure 14**a). The pressure sensor could be used for a wide range of tactile sensing from 250 Pa to 3 MPa, thus providing great potential in diverse applications such as medical diagnosis, robotics, and automotive electronics. Figure 14b showed the integrated array with 28 pressure-sensitive FETs in total within the device size of 2×2 cm^2. The sensor density could be further improved to 50×50 pixels on 2.5×2.5 cm^2 with the resolution of 400 μm, which was mainly determined by the patterning feature size of photo-patternable PDMS as shown in the inset of Figure 14c. The mapping of pressure distribution responded to a tripod-shaped pressing machine exhibited a distinct color gradation contour plot of the resultant signals. Each FET of the high-density arrays could be worked as an independent sensor solely with no accessional component or layer. The device structure was beneficial to the further improvement of pixel resolutions for the active matrix by reducing the FET size. The high resolution confirmed substantial promise in the integration of the graphene-based pressure FETs and other functional electronic elements such as display panels or power-storage devices for next-generation electronics.

Employing CNT/rGO composite nanofibers, Someya and co-workers[57] reported a remarkable approach to fabricate ultraflexible, optically transparent, and piezoresistive pressure sensor arrays with extraordinarily small bending sensitive. As presented in Figure 14d, the fabricated 12×12 ultrathin pressure sensor matrix owned a total thickness of 8 μm after integrating the nanofiber sensors with an active matrix of 2 μm thickness, which minimized the rigidity and enhanced the conformability. The fully integrated devices could be wrapped around an injection needle with a bending radius of 1 mm as displayed in Figure 14e. The performance variations were proved to be negligibly small toward the bending-induced strain, which retaining a high sensitivity and outstanding conformability to external 3D structures. The sensors' matrix could also be attached on the surface of human skin or other soft movable 3D surface to precisely monitor the pressure distribution, which showed a negligibly small crosstalk due to the 1 mm spacing between sensor arrays. Figure 14f,g revealed the capability to detect the pressure distribution on a very soft surface of a balloon while it was being pressed by fingers. It exhibited no imprecision induced by complex mechanical deformations including bending, wrinkling, and twisting. The excellent performance of large-area, normal

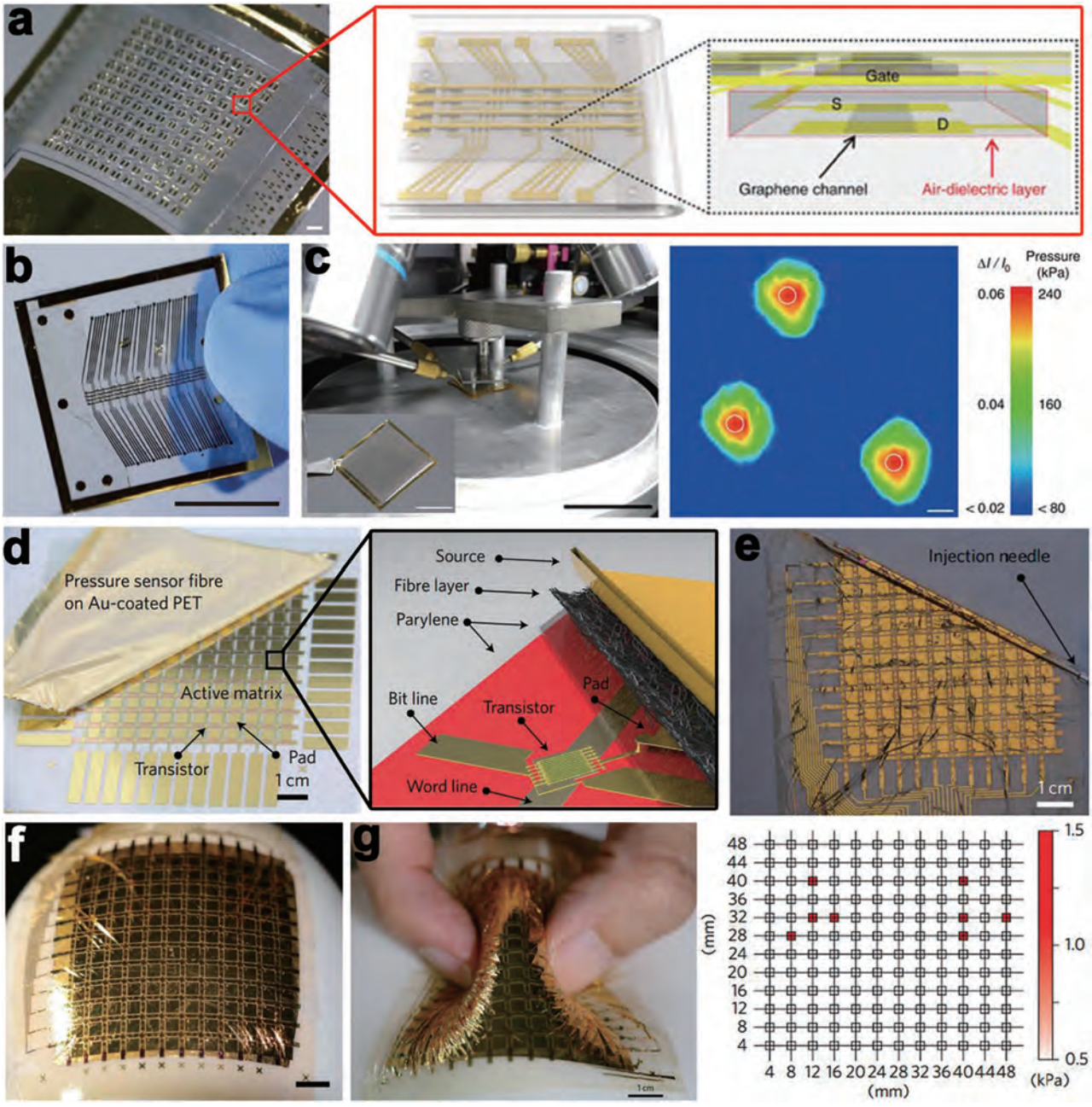

Figure 14. Large-area-integrated E-skin arrays for spatial tactile mapping. a) A flexible active matrix FET array with 12 × 12 pixels and the unit structure of the graphene FETs with air–dielectric layers. b) The fabricated graphene FETs to sense pressure. c) The ability to map tactile distribution while external pressures were applied on the 50 × 50 FET sensor array. (a–c) Reproduced with permission.[196] Copyright 2017, Nature Publishing Group. d) The 12 × 12 arrays integration of CNT/graphene-based pressure sensors with organic-transistor-driven active matrix. e,f) The sensor arrays could be fully wrapped around an injection needle and free-attached to a soft balloon. g) The ability to distribute pressure area while a pressure was applied to the integrated sensor array by a pinching motion. (d–g) Reproduced with permission.[57] Copyright 2016, Macmillan Publishers Ltd.

pressure monitoring under complex conditions for the pressure sensor arrays inspires other clinical and health-monitoring applications such as in situ digital monitoring of diagnosis for breast cancer. However, the spatiotemporal resolution and feasibility of clinical application are required for further improvement.

5. Conclusions and Outlook

Since the discovery of graphene, there are many studies on graphene-based E-skins including flexible and stretchable pressure, temperature, humidity sensors, owing to the excellent mechanical, electrical, and chemical behaviors of graphene.

Graphene-based E-skins are desired for miscellaneous wearable and portable electronic devices such as multifunctional biomimetic E-skins, health and motion monitoring, interactive human–machine interface, and large area integrated E-skins. We expect that further investigation about graphene-based E-skins will be continued, because the development trend of flexible electronics becomes more and more significant in emerging, but burgeoning, electronic applications. In this review, we systematically present a recent progress in graphene-based E-skins including the fabrication of graphene, the sensing mechanism of various functional sensors, and the potential applications of graphene-based E-skins. The massive publications and reports on the topic of graphene-based E-skins demonstrated the insistent demands for future flexible electronics.

Although considerable progress in graphene-based E-skin has been achieved, there are also enormous challenges still remained for future practical applications. The existing problems and future directions are as follows: (1) sensing performance with acceptable working lifetime still requires improvement. The lifetime of functional devices, which is related to the device durability, mechanical and chemical stability, should be enhanced for the actual realization of biomimetic E-skins. Discovering more stable device structures with the ability of self-healing and high stretchability based on porous or honeycomb graphene may be one of the future research directions. (2) The efficient strategy to achieve low-cost construction of E-skin with high performance is desired. In view of recent approaches, to fabricate sensor devices is mostly expensive and complicated; the cost-effective, large-area, and easy-fabrication methods such as flexible printing technology may be a research hotspot in the future. However, the sensing performance of printed devices should be improved due to the immature technique. (3) More attractive properties are required to endow E-skins in order to expand the scope of hodiernal applications. For instance, biologically inspired natures of self-healing, biodegradability, and biocompatibility are expected in the implantable medical devices and physiological monitoring devices, in order to avert an invasive healthcare approach. Besides, some functions that human skin does not possess, such as the ability to sense environmental pollutants, body fluid, and medical biomarkers, are also necessary for more consummate applications. However, researches about these aspects are too few, thus restraining the further development in practical application. (4) The self-power capability is beneficial for wearable E-skin with low energy consumption. For the self-powered systems integrated with functional devices, the energy harvester and energy storage play vital roles in the stable and continuous work of the whole integrated system. In order to acquire a much longer working time, new materials and device structures should be developed to improve the energy and power densities. (5) The high-level large-area integration of the E-skin system is an urgent topic. Flexible sensory electronic devices and integrated circuits should keep abreast with the development of large-area E-skins to meet the demands of applications in advanced robotics, interactive human–machine interface, healthcare monitoring, and implantable medical devices. Overall, graphene has been proved as a feasible material to fabricate wearable E-skins with multifunctional sensing and holds great potential in future applications such as personalized healthcare monitoring, artificial intelligence, and biomimetic flexible electronics.

Acknowledgements

This work was supported by the National Natural Science Foundation of China (Grant Nos. 61625404, 51672308, 61574132, and 61504136), Beijing Natural Science Foundation (Grant No. 4162062), and the Key Research Program of Frontier Sciences, CAS (QYZDY-SSW-JWC004).

Keywords

electronic skins, flexible electronics, graphene, healthcare monitoring, tactile sensors

Received: September 12, 2017
Revised: November 19, 2017
Published online:

[1] W. Gao, S. Emaminejad, H. Y. Nyein, S. Challa, K. Chen, A. Peck, H. M. Fahad, H. Ota, H. Shiraki, D. Kiriya, D. H. Lien, G. A. Brooks, R. W. Davis, A. Javey, *Nature* **2016**, *529*, 509.
[2] C. Larson, B. Peele, S. Li, S. Robinson, M. Totaro, L. Beccai, B. Mazzolai, R. Shepherd, *Science* **2016**, *351*, 1071.
[3] X. Wang, L. Dong, H. Zhang, R. Yu, C. Pan, Z. L. Wang, *Adv. Sci.* **2015**, *2*, 1500169.
[4] R. C. Webb, A. P. Bonifas, A. Behnaz, Y. Zhang, K. J. Yu, H. Cheng, M. Shi, Z. Bian, Z. Liu, Y. S. Kim, W. H. Yeo, J. S. Park, J. Song, Y. Li, Y. Huang, A. M. Gorbach, J. A. Rogers, *Nat. Mater.* **2013**, *12*, 938.
[5] M. L. Hammock, A. Chortos, B. C. Tee, J. B. Tok, Z. Bao, *Adv. Mater.* **2013**, *25*, 5997.
[6] Z. Lei, Q. Wang, S. Sun, W. Zhu, P. Wu, *Adv. Mater.* **2017**, *29*, 1700321.
[7] S. Yang, Y. C. Chen, L. Nicolini, P. Pasupathy, J. Sacks, B. Su, R. Yang, D. Sanchez, Y. F. Chang, P. Wang, D. Schnyer, D. Neikirk, N. Lu, *Adv. Mater.* **2015**, *27*, 6423.
[8] G. A. T. Sevilla, M. D. Cordero, J. M. Nassar, A. N. Hanna, A. T. Kutbee, A. Arevalo, M. M. Hussain, *Adv. Mater. Technol.* **2017**, *2*, 1600175.
[9] S. Zhao, R. Zhu, *Adv. Mater.* **2017**, *29*, 1606151.
[10] T. Q. Trung, N. E. Lee, *Adv. Mater.* **2016**, *28*, 4338.
[11] Z. Liu, J. Xu, D. Chen, G. Shen, *Chem. Soc. Rev.* **2015**, *44*, 161.
[12] T. Yang, D. Xie, Z. Li, H. Zhu, *Mater. Sci. Eng., R* **2017**, *115*, 1.
[13] F. W. Clippinger, R. Avery, B. R. Titus, *Bull. Prosthet. Res.* **1974**, *10*, 247.
[14] V. J. Lumelsky, M. S. Shur, S. Wagner, *IEEE Sens. J.* **2001**, *1*, 41.
[15] S. Jung, J. Lee, T. Hyeon, M. Lee, D. H. Kim, *Adv. Mater.* **2014**, *26*, 6329.
[16] W. Tang, T. Yan, J. Ping, J. Wu, Y. Ying, *Adv. Mater. Technol.* **2017**, *2*, 1700021.
[17] J. He, R. G. Nuzzo, J. A. Rogers, *Proc. IEEE* **2015**, *103*, 619.
[18] C. Lee, Y. Ma, K. I. Jang, A. Banks, T. Pan, X. Feng, J. S. Kim, D. Kang, M. S. Raj, B. L. McGrane, B. Morey, X. Wang, R. Ghaffari, Y. Huang, J. A. Rogers, *Adv. Funct. Mater.* **2015**, *25*, 3698.
[19] X. D. Chen, *Small Methods* **2017**, *1*, 1600029.
[20] K. Takei, T. Takahashi, J. C. Ho, H. Ko, A. G. Gillies, P. W. Leu, R. S. Fearing, A. Javey, *Nat. Mater.* **2010**, *9*, 821.
[21] C. Wang, D. Hwang, Z. Yu, K. Takei, J. Park, T. Chen, B. Ma, A. Javey, *Nat. Mater.* **2013**, *12*, 899.

[22] D. H. Kim, J. Song, W. M. Choi, H. S. Kim, R. H. Kim, Z. Liu, Y. Y. Huang, K. C. Hwang, Y. W. Zhang, J. A. Rogers, *Proc. Natl. Acad. Sci. USA* **2008**, *105*, 18675.
[23] D. H. Kim, J. H. Ahn, W. M. Choi, H. S. Kim, T. H. Kim, J. Song, Y. Y. Huang, Z. Liu, C. Lu, J. A. Rogers, *Science* **2008**, *320*, 507.
[24] T. Someya, Y. Kato, T. Sekitani, S. Iba, Y. Noguchi, Y. Murase, H. Kawaguchi, T. Sakurai, *Proc. Natl. Acad. Sci. USA* **2005**, *102*, 12321.
[25] S. C. Mannsfeld, B. C. Tee, R. M. Stoltenberg, C. V. Chen, S. Barman, B. V. Muir, A. N. Sokolov, C. Reese, Z. Bao, *Nat. Mater.* **2010**, *9*, 859.
[26] B. C. Tee, C. Wang, R. Allen, Z. Bao, *Nat. Nanotechnol.* **2012**, *7*, 825.
[27] J. Y. Oh, S. Rondeau-Gagne, Y. C. Chiu, A. Chortos, F. Lissel, G. N. Wang, B. C. Schroeder, T. Kurosawa, J. Lopez, T. Katsumata, J. Xu, C. Zhu, X. Gu, W. G. Bae, Y. Kim, L. Jin, J. W. Chung, J. B. Tok, Z. Bao, *Nature* **2016**, *539*, 411.
[28] Y. Zang, F. Zhang, C. A. Di, D. Zhu, *Mater. Horiz.* **2015**, *2*, 140.
[29] R. Feiner, L. Engel, S. Fleischer, M. Malki, I. Gal, A. Shapira, Y. Shacham-Diamand, T. Dvir, *Nat. Mater.* **2016**, *15*, 679.
[30] S. Kang, J. Lee, S. Lee, S. Kim, J. Kim, H. Algadi, S. Al-Sayari, D. Kim, D. Kim, T. Lee, *Adv. Electron. Mater.* **2016**, *2*, 1600356.
[31] C. Pang, J. H. Koo, A. Nguyen, J. M. Caves, M. G. Kim, A. Chortos, K. Kim, P. J. Wang, J. B. Tok, Z. Bao, *Adv. Mater.* **2015**, *27*, 634.
[32] L. Pan, A. Chortos, G. Yu, Y. Wang, S. Isaacson, R. Allen, Y. Shi, R. Dauskardt, Z. Bao, *Nat. Commun.* **2014**, *5*, 3002.
[33] S. Y. Kim, S. Park, H. W. Park, D. H. Park, Y. Jeong, D. H. Kim, *Adv. Mater.* **2015**, *27*, 4178.
[34] D. H. Ho, Q. Sun, S. Y. Kim, J. T. Han, H. Kim do, J. H. Cho, *Adv. Mater.* **2016**, *28*, 2601.
[35] X. Wang, Z. Liu, T. Zhang, *Small* **2017**, *13*, 1602790.
[36] J. M. Nassar, K. Mishra, K. Lau, A. A. Aguirre-Pablo, M. M. Hussain, *Adv. Mater. Technol.* **2017**, *2*, 1600228.
[37] W. Xi, J. C. Yeo, L. Yu, S. Zhang, C. T. Lim, *Adv. Mater. Technol.* **2017**, *2*, 1700016.
[38] C. M. Boutry, A. Nguyen, Q. O. Lawal, A. Chortos, S. Rondeau-Gagne, Z. Bao, *Adv. Mater.* **2015**, *27*, 6954.
[39] M. D. Ho, Y. Ling, L. W. Yap, Y. Wang, D. Dong, Y. Zhao, W. Cheng, *Adv. Funct. Mater.* **2017**, *27*, 1700845.
[40] S. Chen, Z. Lou, D. Chen, Z. Chen, K. Jiang, G. Z. Shen, *Sci. China Mater.* **2016**, *59*, 173.
[41] S. Chen, Z. Lou, D. Chen, K. Jiang, G. Z. Shen, *Adv. Mater. Technol.* **2016**, *1*, 1600136.
[42] M. Park, Y. J. Park, X. Chen, Y. K. Park, M. S. Kim, J. H. Ahn, *Adv. Mater.* **2016**, *28*, 2556.
[43] S. Gong, D. T. Lai, Y. Wang, L. W. Yap, K. J. Si, Q. Shi, N. N. Jason, T. Sridhar, H. Uddin, W. Cheng, *ACS Appl. Mater. Interfaces* **2015**, *7*, 19700.
[44] H. Wang, Y. Wang, B. C. Tee, K. Kim, J. Lopez, W. Cai, Z. Bao, *Adv. Sci.* **2015**, *2*, 1500103.
[45] S. Gong, W. Cheng, *Adv. Electron. Mater.* **2017**, *3*, 1600314.
[46] A. K. Geim, *Science* **2009**, *324*, 1530.
[47] H. Y. Mao, S. Laurent, W. Chen, O. Akhavan, M. Imani, A. A. Ashkarran, M. Mahmoudi, *Chem. Rev.* **2013**, *113*, 3407.
[48] B. Saha, S. Baek, J. Lee, *ACS Appl. Mater. Interfaces* **2017**, *9*, 4658.
[49] X. Liu, D. Chao, Y. Li, J. Hao, X. Liu, J. Zhao, J. Lin, H. J. Fan, Z. X. Shen, *Nano Energy* **2015**, *17*, 43.
[50] H. Ota, S. Emaminejad, Y. Gao, A. Zhao, E. Wu, S. Challa, K. Chen, H. M. Fahad, A. K. Jha, D. Kiriya, W. Gao, H. Shiraki, K. Morioka, A. R. Ferguson, K. E. Healy, R. W. Davis, A. Javey, *Adv. Mater. Technol.* **2016**, *1*, 1600013.
[51] T. Li, L. Li, H. Sun, Y. Xu, X. Wang, H. Luo, Z. Liu, T. Zhang, *Adv. Sci.* **2017**, *4*, 1600404.
[52] Q. Zhang, L. Tan, Y. Chen, T. Zhang, W. Wang, Z. Liu, L. Fu, *Adv. Sci.* **2016**, *3*, 1600130.
[53] S. Gong, W. Schwalb, Y. Wang, Y. Chen, Y. Tang, J. Si, B. Shirinzadeh, W. Cheng, *Nat. Commun.* **2014**, *5*, 3132.
[54] T. Yamada, Y. Hayamizu, Y. Yamamoto, Y. Yomogida, A. Izadi-Najafabadi, D. N. Futaba, K. Hata, *Nat. Nanotechnol.* **2011**, *6*, 296.
[55] S. Lim, D. Son, J. Kim, Y. B. Lee, J. K. Song, S. Choi, D. J. Lee, J. H. Kim, M. Lee, T. Hyeon, D. H. Kim, *Adv. Funct. Mater.* **2015**, *25*, 375.
[56] J. Kim, M. Lee, H. J. Shim, R. Ghaffari, H. R. Cho, D. Son, Y. H. Jung, M. Soh, C. Choi, S. Jung, K. Chu, D. Jeon, S. T. Lee, J. H. Kim, S. H. Choi, T. Hyeon, D. H. Kim, *Nat. Commun.* **2014**, *5*, 5747.
[57] S. Lee, A. Reuveny, J. Reeder, S. Lee, H. Jin, Q. Liu, T. Yokota, T. Sekitani, T. Isoyama, Y. Abe, Z. Suo, T. Someya, *Nat. Nanotechnol.* **2016**, *11*, 472.
[58] K. S. Novoselov, A. K. Geim, S. V. Morozov, D. Jiang, Y. Zhang, S. V. Dubonos, I. V. Grigorieva, A. A. Firsov, *Science* **2004**, *306*, 666.
[59] G. Zhao, X. Li, M. Huang, Z. Zhen, Y. Zhong, Q. Chen, X. Zhao, Y. He, R. Hu, T. Yang, R. Zhang, C. Li, J. Kong, J. B. Xu, R. S. Ruoff, H. Zhu, *Chem. Soc. Rev.* **2017**, *46*, 4417.
[60] Y. Zheng, H. Wang, S. Hou, D. Xia, *Adv. Mater. Technol.* **2017**, *2*, 1600237.
[61] H. He, W. Fu, H. Wang, H. Wang, C. Jin, H. J. Fan, Z. Liu, *Nano Energy* **2017**, *34*, 449.
[62] C. Yan, J. H. Cho, J. H. Ahn, *Nanoscale* **2012**, *4*, 4870.
[63] S. K. Lee, K. Rana, J. H. Ahn, *J. Phys. Chem. Lett.* **2013**, *4*, 831.
[64] K. S. Kim, H. J. Lee, C. Lee, S. K. Lee, H. Jang, J. H. Ahn, J. H. Kim, H. J. Lee, *ACS Nano* **2011**, *5*, 5107.
[65] J. U. Park, S. Nam, M. S. Lee, C. M. Lieber, *Nat. Mater.* **2011**, *11*, 120.
[66] B. Jang, C. H. Kim, S. T. Choi, K. S. Kim, K. S. Kim, H. J. Lee, S. Cho, J. H. Ahn, J. H. Kim, *2D Mater.* **2017**, *4*, 024002.
[67] Y. J. Kim, S. J. Kim, M. H. Jung, K. Y. Choi, S. Bae, S. K. Lee, Y. Lee, D. Shin, B. Lee, H. Shin, M. Choi, K. Park, J. H. Ahn, B. H. Hong, *Nanotechnology* **2012**, *23*, 344016.
[68] J. Ryu, Y. Kim, D. Won, N. Kim, J. S. Park, E. K. Lee, D. Cho, S. P. Cho, S. J. Kim, G. H. Ryu, H. A. Shin, Z. Lee, B. H. Hong, S. Cho, *ACS Nano* **2014**, *8*, 950.
[69] J. Wang, M. Zeng, L. Tan, B. Dai, Y. Deng, M. Rummeli, H. Xu, Z. Li, S. Wang, L. Peng, J. Eckert, L. Fu, *Sci. Rep.* **2013**, *3*, 2670.
[70] M. Zeng, L. Tan, J. Wang, L. Chen, M. H. Rümmeli, L. Fu, *Chem. Mater.* **2014**, *26*, 3637.
[71] A. Reina, X. Jia, J. Ho, D. Nezich, H. Son, V. Bulovic, M. S. Dresselhaus, J. Kong, *Nano Lett.* **2009**, *9*, 30.
[72] B. N. Chandrashekar, B. Deng, A. S. Smitha, Y. Chen, C. Tan, H. Zhang, H. Peng, Z. Liu, *Adv. Mater.* **2015**, *27*, 5210.
[73] Y. Liu, B. Weng, Q. H. Xu, Y. Hou, C. Zhao, S. Beirne, K. Shu, R. Jalili, G. G. Wallace, J. M. Razal, J. Chen, *Adv. Mater. Technol.* **2016**, *1*, 1600166.
[74] S. Bae, H. Kim, Y. Lee, X. Xu, J. S. Park, Y. Zheng, J. Balakrishnan, T. Lei, H. R. Kim, Y. I. Song, Y. J. Kim, K. S. Kim, B. Ozyilmaz, J. H. Ahn, B. H. Hong, S. Iijima, *Nat. Nanotechnol.* **2010**, *5*, 574.
[75] J. Kang, S. Hwang, J. H. Kim, M. H. Kim, J. Ryu, S. J. Seo, B. H. Hong, M. K. Kim, J. B. Choi, *ACS Nano* **2012**, *6*, 5360.
[76] G. Eda, G. Fanchini, M. Chhowalla, *Nat. Nanotechnol.* **2008**, *3*, 270.
[77] V. C. Tung, M. J. Allen, Y. Yang, R. B. Kaner, *Nat. Nanotechnol.* **2009**, *4*, 25.
[78] M. Michel, C. Biswas, C. S. Tiwary, G. A. Saenz, R. F. Hossain, P. M. Ajayan, A. B. Kaul, *2D Mater.* **2017**, *4*, 025076.
[79] H. J. Shin, K. K. Kim, A. Benayad, S. M. Yoon, H. K. Park, I. S. Jung, M. H. Jin, H. K. Jeong, J. M. Kim, J. Y. Choi, Y. H. Lee, *Adv. Funct. Mater.* **2009**, *19*, 1987.
[80] O. Akhavan, *Carbon* **2010**, *48*, 509.

[81] W. Chen, L. Yan, P. R. Bangal, *Carbon* **2010**, *48*, 1146.
[82] L. Peng, Z. Xu, Z. Liu, Y. Wei, H. Sun, Z. Li, X. Zhao, C. Gao, *Nat. Commun.* **2015**, *6*, 5716.
[83] S. Pei, H. M. Cheng, *Carbon* **2012**, *50*, 3210.
[84] S. Stankovich, D. A. Dikin, G. H. Dommett, K. M. Kohlhaas, E. J. Zimney, E. A. Stach, R. D. Piner, S. T. Nguyen, R. S. Ruoff, *Nature* **2006**, *442*, 282.
[85] R. R. Nair, P. Blake, A. N. Grigorenko, K. S. Novoselov, T. J. Booth, T. Stauber, N. M. Peres, A. K. Geim, *Science* **2008**, *320*, 1308.
[86] J. Wang, M. Liang, Y. Fang, T. Qiu, J. Zhang, L. Zhi, *Adv. Mater.* **2012**, *24*, 2874.
[87] D. A. Dikin, S. Stankovich, E. J. Zimney, R. D. Piner, G. H. Dommett, G. Evmenenko, S. T. Nguyen, R. S. Ruoff, *Nature* **2007**, *448*, 457.
[88] J. Wu, J. Yang, Y. Huang, H. Li, Z. Fan, J. Liu, X. Cao, X. Huang, W. Huang, H. Zhang, *Adv. Mater. Technol.* **2017**, *2*, 1600231.
[89] I. Jung, D. A. Dikin, R. D. Piner, R. S. Ruoff, *Nano Lett.* **2008**, *8*, 4283.
[90] L. L. Wang, J. A. Jackman, W. B. Ng, N. J. Cho, *Adv. Funct. Mater.* **2016**, *26*, 8623.
[91] L. Tao, D. Y. Wang, S. Jiang, Y. Liu, Q. Y. Xie, H. Tian, N. Deng, X. Wang, Y. Yang, T. L. Ren, *J. Semicond.* **2016**, *37*, 041001.
[92] L. L. Wang, W. B. Ng, J. A. Jackman, N. J. Cho, *Adv. Funct. Mater.* **2016**, *26*, 2097.
[93] Q. Li, Z. Ullah, W. Li, Y. Guo, J. Xu, R. Wang, Q. Zeng, M. Chen, C. Liu, L. Liu, *Small* **2016**, *12*, 5058.
[94] M. S. Lee, K. Lee, S. Y. Kim, H. Lee, J. Park, K. H. Choi, H. K. Kim, D. G. Kim, D. Y. Lee, S. Nam, J. U. Park, *Nano Lett.* **2013**, *13*, 2814.
[95] P. Sun, K. Wang, H. Zhu, *Adv. Mater.* **2016**, *28*, 2287.
[96] K. Vimalanathan, C. L. Raston, *Adv. Mater. Technol.* **2017**, *2*, 1600298.
[97] W. Chen, X. Gui, B. Liang, R. Yang, Y. Zheng, C. Zhao, X. Li, H. Zhu, Z. Tang, *ACS Appl. Mater. Interfaces* **2017**, *9*, 24111.
[98] S. Chun, Y. Choi, W. Park, *Carbon* **2017**, *116*, 753.
[99] H. Song, J. Zhang, D. Chen, K. Wang, S. Niu, Z. Han, L. Ren, *Nanoscale* **2017**, *9*, 1166.
[100] X. Fu, Z. Liao, J. Zhou, Y. Zhou, H. Wu, R. Zhang, G. Jing, J. Xu, X. Wu, W. Guo, D. Yu, *Appl. Phys. Lett.* **2011**, *99*, 213107.
[101] Y. Wang, R. Yang, Z. Shi, L. Zhang, D. Shi, E. Wang, G. Zhang, *ACS Nano* **2011**, *5*, 3645.
[102] Z. Chen, W. Ren, L. Gao, B. Liu, S. Pei, H. M. Cheng, *Nat. Mater.* **2011**, *10*, 424.
[103] L. Qiu, J. Z. Liu, S. L. Chang, Y. Wu, D. Li, *Nat. Commun.* **2012**, *3*, 1241.
[104] H. B. Yao, J. Ge, C. F. Wang, X. Wang, W. Hu, Z. J. Zheng, Y. Ni, S. H. Yu, *Adv. Mater.* **2013**, *25*, 6692.
[105] C. Yan, J. Wang, W. Kang, M. Cui, X. Wang, C. Y. Foo, K. J. Chee, P. S. Lee, *Adv. Mater.* **2014**, *26*, 2022.
[106] Y. Cheng, R. Wang, J. Sun, L. Gao, *Adv. Mater.* **2015**, *27*, 7365.
[107] S. Chun, A. Hong, Y. Choi, C. Ha, W. Park, *Nanoscale* **2016**, *8*, 9185.
[108] S. Wan, H. Bi, Y. Zhou, X. Xie, S. Su, K. Yin, L. Sun, *Carbon* **2017**, *114*, 209.
[109] T. Y. Choi, B. U. Hwang, B. Y. Kim, T. Q. Trung, Y. H. Nam, D. N. Kim, K. Eom, N. E. Lee, *ACS Appl. Mater. Interfaces* **2017**, *9*, 18022.
[110] J. Park, M. Kim, Y. Lee, H. S. Lee, H. Ko, *Sci. Adv.* **2015**, *1*, e1500661.
[111] Z. Chen, Z. Wang, X. Li, Y. Lin, N. Luo, M. Long, N. Zhao, J. B. Xu, *ACS Nano* **2017**, *11*, 4507.
[112] J. Kuang, Z. Dai, L. Liu, Z. Yang, M. Jin, Z. Zhang, *Nanoscale* **2015**, *7*, 9252.
[113] M. N. Tsui, M. F. Islam, *Nanoscale* **2017**, *9*, 1128.
[114] Y. W. Choi, D. Kang, P. V. Pikhitsa, T. Lee, S. M. Kim, G. Lee, D. Tahk, M. Choi, *Sci. Rep.* **2017**, *7*, 40116.
[115] M. A. S. M. Haniff, S. M. Hafiz, K. A. A. Wahid, Z. Endut, H. W. Lee, D. C. Bien, I. A. Azid, M. Z. Abdullah, N. M. Huang, S. A. Rahman, *Sci. Rep.* **2015**, *5*, 14751.
[116] H. Tian, Y. Shu, X. F. Wang, M. A. Mohammad, Z. Bie, Q. Y. Xie, C. Li, W. T. Mi, Y. Yang, T. L. Ren, *Sci. Rep.* **2015**, *5*, 8603.
[117] Y. A. Samad, K. Komatsu, D. Yamashita, Y. Li, L. Zheng, S. M. Alhassan, Y. Nakano, K. Liao, *Sens. Actuators, B* **2017**, *240*, 1083.
[118] X. H. Xia, D. L. Chao, Y. Q. Zhang, Z. X. Shen, H. J. Fan, *Nano Today* **2014**, *9*, 785.
[119] S. Liu, X. Wu, D. Zhang, C. Guo, P. Wang, W. Hu, X. Li, X. Zhou, H. Xu, C. Luo, J. Zhang, J. Chu, *ACS Appl. Mater. Interfaces* **2017**, *9*, 24148.
[120] C. S. Boland, U. Khan, C. Backes, A. O'Neill, J. McCauley, S. Duane, R. Shanker, Y. Liu, I. Jurewicz, A. B. Dalton, J. N. Coleman, *ACS Nano* **2014**, *8*, 8819.
[121] S. Wu, R. B. Ladani, J. Zhang, K. Ghorbani, X. Zhang, A. P. Mouritz, A. J. Kinloch, C. H. Wang, *ACS Appl. Mater. Interfaces* **2016**, *8*, 24853.
[122] Z. Lou, S. Chen, L. Wang, K. Jiang, G. Z. Shen, *Nano Energy* **2016**, *23*, 7.
[123] G. Y. Bae, S. W. Pak, D. Kim, G. Lee, H. Kim do, Y. Chung, K. Cho, *Adv. Mater.* **2016**, *28*, 5300.
[124] M. Jian, K. Xia, Q. Wang, Z. Yin, H. Wang, C. Wang, H. Xie, M. Zhang, Y. Zhang, *Adv. Funct. Mater.* **2017**, *27*, 1606066.
[125] H. Liu, M. Dong, W. Huang, J. Gao, K. Dai, J. Guo, G. Zheng, C. Liu, C. Shen, Z. Guo, *J. Mater. Chem. C* **2017**, *5*, 73.
[126] J. Sha, Y. Li, R. Villegas Salvatierra, T. Wang, P. Dong, Y. Ji, S. K. Lee, C. Zhang, J. Zhang, R. H. Smith, P. M. Ajayan, J. Lou, N. Zhao, J. M. Tour, *ACS Nano* **2017**, *11*, 6860.
[127] Y. Pang, H. Tian, L. Tao, Y. Li, X. Wang, N. Deng, Y. Yang, T. L. Ren, *ACS Appl. Mater. Interfaces* **2016**, *8*, 26458.
[128] L. Lv, P. Zhang, T. Xu, L. Qu, *ACS Appl. Mater. Interfaces* **2017**, *9*, 22885.
[129] Y. A. Samad, Y. Li, A. Schiffer, S. M. Alhassan, K. Liao, *Small* **2015**, *11*, 2380.
[130] X. Xu, R. Wang, P. Nie, Y. Cheng, X. Lu, L. Shi, J. Sun, *ACS Appl. Mater. Interfaces* **2017**, *9*, 14273.
[131] S. Jung, J. H. Kim, J. Kim, S. Choi, J. Lee, I. Park, T. Hyeon, D. H. Kim, *Adv. Mater.* **2014**, *26*, 4825.
[132] X. Li, T. Hua, B. Xu, *Carbon* **2017**, *118*, 686.
[133] D. Hu, Q. Wang, J. Yu, W. Hao, H. Lu, G. Zhang, X. Wang, L. Qiu, *J. Nanosci. Nanotechnol.* **2016**, *16*, 5839.
[134] J. J. Park, W. J. Hyun, S. C. Mun, Y. T. Park, O. O. Park, *ACS Appl. Mater. Interfaces* **2015**, *7*, 6317.
[135] C. Wang, X. Li, E. Gao, M. Jian, K. Xia, Q. Wang, Z. Xu, T. Ren, Y. Zhang, *Adv. Mater.* **2016**, *28*, 6640.
[136] B. Nie, R. Li, J. Cao, J. D. Brandt, T. Pan, *Adv. Mater.* **2015**, *27*, 6055.
[137] M. Habibi, S. Darbari, S. Rajabali, V. Ahmadi, *Carbon* **2016**, *96*, 259.
[138] V. Mitrakos, L. Macintyre, F. Denison, P. Hands, M. Desmulliez, *Micromachines* **2017**, *8*, 41.
[139] Y. M. Chen, S. M. He, C. H. Huang, C. C. Huang, W. P. Shih, C. L. Chu, J. Kong, J. Li, C. Y. Su, *Nanoscale* **2016**, *8*, 3555.
[140] D. J. Lipomi, M. Vosgueritchian, B. C. Tee, S. L. Hellstrom, J. A. Lee, C. H. Fox, Z. Bao, *Nat. Nanotechnol.* **2011**, *6*, 788.
[141] Y. F. Ai, Z. Lou, L. Li, S. Chen, H. S. Park, Z. M. Wang, G. Z. Shen, *Adv. Mater. Technol.* **2016**, *1*, 1600142.
[142] L. Li, Z. Lou, W. Han, D. Chen, K. Jiang, G. Z. Shen, *Adv. Mater. Technol.* **2017**, *2*, 1600282.
[143] J. Liu, D. Galpaya, M. Notarianni, C. Yan, N. Motta, *Appl. Phys. Lett.* **2013**, *103*, 063108.
[144] C. Gomez-Navarro, R. T. Weitz, A. M. Bittner, M. Scolari, A. Mews, M. Burghard, K. Kern, *Nano Lett.* **2007**, *7*, 3499.

[145] Q. Tang, P. Yang, *J. Mater. Chem. A* **2016**, *4*, 9730.
[146] S. Garain, S. Jana, T. K. Sinha, D. Mandal, *ACS Appl. Mater. Interfaces* **2016**, *8*, 4532.
[147] H. Chen, Y. Xu, L. Bai, Y. Jiang, J. Zhang, C. Zhao, T. Li, H. Yu, G. Song, N. Zhang, Q. Gan, *Adv. Mater. Technol.* **2017**, *2*, 1700044.
[148] D. Chao, C. Zhu, X. Xia, J. Liu, X. Zhang, J. Wang, P. Liang, J. Lin, H. Zhang, Z. X. Shen, H. J. Fan, *Nano Lett.* **2015**, *15*, 565.
[149] L. Persano, C. Dagdeviren, Y. Su, Y. Zhang, S. Girardo, D. Pisignano, Y. Huang, J. A. Rogers, *Nat. Commun.* **2013**, *4*, 1633.
[150] M. Huang, T. A. Pascal, H. Kim, W. A. Goddard, J. R. Greer, *Nano Lett.* **2011**, *11*, 1241.
[151] K. Xu, K. Wang, W. Zhao, W. Bao, E. Liu, Y. Ren, M. Wang, Y. Fu, J. Zeng, Z. Li, W. Zhou, F. Song, X. Wang, Y. Shi, X. Wan, M. S. Fuhrer, B. Wang, Z. Qiao, F. Miao, D. Xing, *Nat. Commun.* **2015**, *6*, 8119.
[152] J. Lao, Y. He, X. Li, F. Wu, T. Yang, M. Zhu, Y. Zhang, P. Sun, Z. Zhen, B. Cheng, H. Zhu, *Nano Res.* **2015**, *8*, 2467.
[153] J. Yin, Z. Zhang, X. Li, J. Yu, J. Zhou, Y. Chen, W. Guo, *Nat. Commun.* **2014**, *5*, 3582.
[154] H. Zhong, J. Xia, F. Wang, H. Chen, H. Wu, S. Lin, *Adv. Funct. Mater.* **2017**, *27*, 1604226.
[155] U. Khan, T. H. Kim, H. Ryu, W. Seung, S. W. Kim, *Adv. Mater.* **2017**, *29*, 1603544.
[156] S. Chen, Y. Wei, X. Yuan, Y. Lin, L. Liu, *J. Mater. Chem. C* **2016**, *4*, 4304.
[157] H. Chu, H. Jang, Y. Lee, Y. Chae, J. H. Ahn, *Nano Energy* **2016**, *27*, 298.
[158] X. Wang, B. Yang, J. Liu, Y. Zhu, C. Yang, Q. He, *Sci. Rep.* **2016**, *6*, 36409.
[159] S. Y. Hong, Y. H. Lee, H. Park, S. W. Jin, Y. R. Jeong, J. Yun, I. You, G. Zi, J. S. Ha, *Adv. Mater.* **2016**, *28*, 930.
[160] X. Ren, K. Pei, B. Peng, Z. Zhang, Z. Wang, X. Wang, P. K. Chan, *Adv. Mater.* **2016**, *28*, 4832.
[161] J. Zhang, G. Liao, S. H. Jin, D. Cao, Q. Wei, H. Lu, J. Yu, X. Cai, S. Tan, Y. Xiao, J. Tang, Y. Luo, Z. Chen, *Laser Phys. Lett.* **2014**, *11*, 035901.
[162] J. Zhu, C. M. Andres, J. Xu, A. Ramamoorthy, T. Tsotsis, N. A. Kotov, *ACS Nano* **2012**, *6*, 8357.
[163] D. Kong, L. T. Le, Y. Li, J. L. Zunino, W. Lee, *Langmuir* **2012**, *28*, 13467.
[164] C. Yan, J. Wang, P. S. Lee, *ACS Nano* **2015**, *9*, 2130.
[165] T. Q. Trung, S. Ramasundaram, B. U. Hwang, N. E. Lee, *Adv. Mater.* **2016**, *28*, 502.
[166] J. J. Bae, S. C. Lim, G. H. Han, Y. W. Jo, D. L. Doung, E. S. Kim, S. J. Chae, T. Q. Huy, N. Van Luan, Y. H. Lee, *Adv. Funct. Mater.* **2012**, *22*, 4819.
[167] H. Yang, D. Qi, Z. Liu, B. K. Chandran, T. Wang, J. Yu, X. Chen, *Adv. Mater.* **2016**, *28*, 9175.
[168] P. Liu, C. X. Liu, Y. Huang, W. H. Wang, D. Fang, Y. G. Zhang, Y. J. Ge, *J. Appl. Polym. Sci.* **2016**, *133*, 42979.
[169] R. Ackerley, H. Olausson, J. Wessberg, F. McGlone, *Neurosci. Lett.* **2012**, *522*, 73.
[170] L. L. Wang, J. A. Jackman, J. H. Park, E. L. Tan, N. J. Cho, *J. Mater. Chem. B* **2017**, *5*, 4019.
[171] S. Borini, R. White, D. Wei, M. Astley, S. Haque, E. Spigone, N. Harris, J. Kivioja, T. Ryhanen, *ACS Nano* **2013**, *7*, 11166.
[172] S. H. Hwang, D. Kang, R. S. Ruoff, H. S. Shin, Y. B. Park, *ACS Nano* **2014**, *8*, 6739.
[173] Z. Chen, C. Lu, *Sens. Lett.* **2005**, *3*, 274.
[174] R. Nohria, R. K. Khillan, Y. Su, R. Dikshit, Y. Lvov, K. Varahramyan, *Sens. Actuators, B* **2006**, *114*, 218.
[175] D. Zhang, J. Tong, B. Xia, Q. Xue, *Sens. Actuators, B* **2014**, *203*, 263.
[176] R. Gao, D. F. Lu, J. Cheng, Y. Jiang, L. Jiang, Z. M. Qi, *Sens. Actuators, B* **2016**, *222*, 618.
[177] D. Zhang, J. Tong, B. Xia, *Sens. Actuators, B* **2014**, *197*, 66.
[178] A. Buchsteiner, A. Lerf, J. Pieper, *J. Phys. Chem. B* **2006**, *110*, 22328.
[179] D. Zhang, H. Chang, P. Li, R. Liu, Q. Xue, *Sens. Actuators, B* **2016**, *225*, 233.
[180] W. D. Lin, H. M. Chang, R. J. Wu, *Sens. Actuators, B* **2013**, *181*, 326.
[181] T. Q. Trung, L. T. Duy, S. Ramasundaram, N. E. Lee, *Nano Res.* **2017**, *10*, 2021.
[182] Q. Kuang, C. Lao, Z. L. Wang, Z. Xie, L. Zheng, *J. Am. Chem. Soc.* **2007**, *129*, 6070.
[183] T. S. Sreeprasad, A. A. Rodriguez, J. Colston, A. Graham, E. Shishkin, V. Pallem, V. Berry, *Nano Lett.* **2013**, *13*, 1757.
[184] H. He, Y. Fu, W. Zang, Q. Wang, L. Xing, Y. Zhang, X. Xue, *Nano Energy* **2017**, *31*, 37.
[185] J. M. Nassar, M. D. Cordero, A. T. Kutbee, M. A. Karimi, G. A. T. Sevilla, A. M. Hussain, A. Shamim, M. M. Hussain, *Adv. Mater. Technol.* **2016**, *1*, 1600004.
[186] W. H. Yeo, Y. S. Kim, J. Lee, A. Ameen, L. Shi, M. Li, S. Wang, R. Ma, S. H. Jin, Z. Kang, Y. Huang, J. A. Rogers, *Adv. Mater.* **2013**, *25*, 2773.
[187] L. Li, Z. Lou, W. Han, G. Shen, *Nanoscale* **2016**, *8*, 14986.
[188] J. C. Yeo, Z. Liu, Z. Q. Zhang, P. Zhang, Z. Wang, C. T. Lim, *Adv. Mater. Technol.* **2017**, *2*, 1700006.
[189] K. Shehzad, T. Shi, A. Qadir, X. Wan, H. Guo, A. Ali, W. Xuan, H. Xu, Z. Gu, X. Peng, J. Xie, L. Sun, Q. He, Z. Xu, C. Gao, Y. S. Rim, Y. Dan, T. Hasan, P. Tan, E. Li, W. Yin, Z. Cheng, B. Yu, Y. Xu, J. Luo, X. Duan, *Adv. Mater. Technol.* **2017**, *2*, 1600262.
[190] D. H. Kim, J. Xiao, J. Song, Y. Huang, J. A. Rogers, *Adv. Mater.* **2010**, *22*, 2108.
[191] N. T. Tien, S. Jeon, D. I. Kim, T. Q. Trung, M. Jang, B. U. Hwang, K. E. Byun, J. Bae, E. Lee, J. B. Tok, Z. Bao, N. E. Lee, J. J. Park, *Adv. Mater.* **2014**, *26*, 796.
[192] C. Jia, Q. Wang, N. Xin, J. Zhou, Y. Gong, L. Li, Q. Sun, X. Guo, *Adv. Mater. Technol.* **2016**, *1*, 1600067.
[193] L. Li, L. Gu, Z. Lou, Z. Fan, G. Shen, *ACS Nano* **2017**, *11*, 4067.
[194] W. Li, J. Guo, D. Fan, *Adv. Mater. Technol.* **2017**, *2*, 1700070.
[195] D. D. Liana, B. Raguse, J. J. Gooding, E. Chow, *Adv. Mater. Technol.* **2016**, *1*, 1600143.
[196] S. H. Shin, S. Ji, S. Choi, K. H. Pyo, B. Wan An, J. Park, J. Kim, J. Y. Kim, K. S. Lee, S. Y. Kwon, J. Heo, B. G. Park, J. U. Park, *Nat. Commun.* **2017**, *8*, 14950.
[197] W. W. Nichols, *Am. J. Hypertens.* **2005**, *18*, 3S.
[198] T. Yang, X. Jiang, Y. Zhong, X. Zhao, S. Lin, J. Li, X. Li, J. Xu, Z. Li, H. Zhu, *ACS Sens.* **2017**, *2*, 967.
[199] L. Q. Tao, H. Tian, Y. Liu, Z. Y. Ju, Y. Pang, Y. Q. Chen, D. Y. Wang, X. G. Tian, J. C. Yan, N. Q. Deng, Y. Yang, T. L. Ren, *Nat. Commun.* **2017**, *8*, 14579.
[200] Q. Sun, W. Seung, B. J. Kim, S. Seo, S. W. Kim, J. H. Cho, *Adv. Mater.* **2015**, *27*, 3411.
[201] N. Luo, W. Dai, C. Li, Z. Zhou, L. Lu, C. C. Y. Poon, S. C. Chen, Y. Zhang, N. Zhao, *Adv. Funct. Mater.* **2016**, *26*, 1178.
[202] Z. Lou, S. Chen, L. Wang, R. Shi, L. Li, K. Jiang, D. Chen, G. Z. Shen, *Nano Energy* **2017**, *38*, 28.
[203] Y. Ai, Z. Lou, S. Chen, D. Chen, Z. M. Wang, K. Jiang, G. Z. Shen, *Nano Energy* **2017**, *35*, 121.
[204] L. Lin, Y. Xie, S. Wang, W. Wu, S. Niu, X. Wen, Z. L. Wang, *ACS Nano* **2013**, *7*, 8266.
[205] J. Mu, C. Hou, H. Wang, Y. Li, Q. Zhang, M. Zhu, *Sci. Adv.* **2015**, *1*, e1500533.
[206] X. Pu, H. Guo, J. Chen, X. Wang, Y. Xi, C. Hu, Z. L. Wang, *Sci. Adv.* **2017**, *3*, e1700694.

[207] R. K. Mishra, L. J. Hubble, A. Martin, R. Kumar, A. Barfidokht, J. Kim, M. M. Musameh, I. L. Kyratzis, J. Wang, *ACS Sens.* **2017**, *2*, 553.
[208] M. Amjadi, A. Pichitpajongkit, S. Lee, S. Ryu, I. Park, *ACS Nano* **2014**, *8*, 5154.
[209] S. Gong, D. T. H. Lai, B. Su, K. J. Si, Z. Ma, L. W. Yap, P. Guo, W. Cheng, *Adv. Electron. Mater.* **2015**, *1*, 1400063.
[210] S. Lee, S. H. Shin, S. Lee, J. Seo, J. Lee, S. Son, H. J. Cho, H. Algadi, S. Al-Sayari, D. E. Kim, T. Lee, *Adv. Funct. Mater.* **2015**, *25*, 3114.
[211] C. G. Núñez, W. T. Navaraj, E. O. Polat, R. Dahiya, *Adv. Funct. Mater.* **2017**, *27*, 1606287.
[212] K. I. Jang, K. Li, H. U. Chung, S. Xu, H. N. Jung, Y. Yang, J. W. Kwak, H. H. Jung, J. Song, C. Yang, A. Wang, Z. Liu, J. Y. Lee, B. H. Kim, J. H. Kim, J. Lee, Y. Yu, B. J. Kim, H. Jang, K. J. Yu, J. Kim, J. W. Lee, J. W. Jeong, Y. M. Song, Y. Huang, Y. Zhang, J. A. Rogers, *Nat. Commun.* **2017**, *8*, 15894.
[213] T. Sekitani, T. Someya, *Adv. Mater.* **2010**, *22*, 2228.
[214] T. Sekitani, Y. Noguchi, K. Hata, T. Fukushima, T. Aida, T. Someya, *Science* **2008**, *321*, 1468.

